Pacific Northwest
NATIONAL LABORATORY

PNNL-36770, Rev. 0

Materials Characterization, Prediction, and Control Project

Characterization of 316L Stainless Steel after Solid Phase Processing using Ultrasonic NDE Method

September 2024

Y Guo
DR Todd
DA Koch
JD Escobar Atehortua
NA Conway
MS Good
M Pole

With contributions from:
K Nwe
DM Brown
C Minerich
D Garcia
T Wang
H Das
KA Ross
EI Barker
LE Smith

U.S. DEPARTMENT OF ENERGY

Prepared for the U.S. Department of Energy
under Contract DE-AC05-76RL01830

DISCLAIMER

PACIFIC NORTHWEST NATIONAL LABORATORY
operated by
BATTELLE
for the
UNITED STATES DEPARTMENT OF ENERGY
under Contract DE-AC05-76RL01830

Printed in the United States of America

Available to DOE and DOE contractors from the
Office of Scientific and Technical Information,
P.O. Box 62, Oak Ridge, TN 37831-0062;
ph: (865) 576-8401
fax: (865) 576-5728
email: reports@adonis.osti.gov

Available to the public from the National Technical Information Service
5301 Shawnee Rd., Alexandria, VA 22312
ph: (800) 553-NTIS (6847)
email: orders@ntis.gov <https://www.ntis.gov/about>
Online ordering: http://www.ntis.gov

Materials Characterization, Prediction, and Control Project

Characterization of 316L Stainless Steel after Solid Phase Processing using Ultrasonic NDE Method

September 2024

Y Guo
DR Todd
DA Koch
JD Escobar Atehortua
NA Conway
MS Good
M Pole

With contributions from:
K Nwe
DM Brown
C Minerich
D Garcia
T Wang
H Das
KA Ross
EI Barker
LE Smith

Prepared for
the U.S. Department of Energy
under Contract DE-AC05-76RL01830

Pacific Northwest National Laboratory
Richland, Washington 99354

Executive Summary

The Pacific Northwest National Laboratory undertook the Materials Characterization, Prediction, and Control Laboratory Directed Research and Development Project to advance understanding of nuclear material processing and enable multifold acceleration in the development and qualification of new material systems produced via advanced manufacturing methods, such as solid phase processing, for use in national security and advanced energy applications (Smith 2021). A motivation of the Materials Characterization, Prediction, and Control Project was to demonstrate ultrasonic testing as a nondestructive evaluation method to complement traditional destructive methods for characterizing material microstructure with emphasis on grain size determination using a method that may have future applications for real-time inline process monitoring.

The objective of the work described in this report is to establish the process and an analysis method for measuring grain sizes of polycrystalline metals with ultrafine grains using ultrasonic shear wave backscattering, building on prior studies on coarser-grained material. The work involves five tasks:

1. Measured ultrasonic backscattering experimentally for a series of 316L stainless steel specimens with various grain sizes made by friction stir processing.
2. Calculated ultrasonic backscattering coefficients from experimental data based on a physical measurement model.
3. Measured ground truth grain sizes of the specimens from electron backscatter diffraction grain boundary images using a generalization of the ASTM E112 (ASTM 2021) intercept method.
4. Built a curve of ultrasonic backscattering coefficients versus the ground truth intercept-based grain sizes to determine the correlation between mean grain sizes and ultrasonic measurements.
5. Demonstrated the ability of using the correlation curve to deduce grain sizes with measured ultrasonic backscattering coefficients for a few 316L stainless steel specimens whose grain sizes were unknown beforehand but were targeted to be an extrapolation to larger grain sizes than used to formulate the correlation curves.

Experimental procedures and computational algorithms are developed and validated for these tasks. This work establishes an ultrasonic technique for characterizing material microstructure with ultrafine grains that are often resulted by solid-phase processing. The technique is nondestructive, and it has the potential to be used for real time inline process monitoring.

This work successfully demonstrates the viability of an ultrasonic nondestructive evaluation method for microstructural characterization of material having ultrafine grain structure (as small as 1 μm) and produced by an advanced manufacturing method. This includes a demonstration of the method to extrapolate to other conditions. While not demonstrated here, the method is expected to be viable for in-line, or near-inline, process monitoring in advanced manufacturing applications with suitable consideration for access of instrumentation to the material being manufactured.

Acknowledgments

This research was supported by the Materials Characterization, Prediction, and Control (MCPC) investment, under the Laboratory Directed Research and Development (LDRD) Program at Pacific Northwest National Laboratory (PNNL). PNNL is a multi-program national laboratory operated for the Department of Energy (DOE) by Battelle Memorial Institute under Contract No. DE-AC05-76RL01830.

Acronyms and Abbreviations

CED	Circle Equivalent Diameter
E2E	End-to-End
EBSD	Electron Backscatter Diffraction
SEM	Scanning Electron Microscope
FOM	Figure-Of-Merit
FS	Fractional Shortening
FSP	Friction Stir Processing
MCPC	Materials Characterization, Prediction, and Control
NDE	Nondestructive Evaluation
rms	root-mean-squared
ShAPE	Shear-Assisted Processing and Extrusion
USB	Universal Serial Bus
UT	Ultrasonic Testing

Contents

Figures

Tables

1.0 Introduction and Background

The Pacific Northwest National Laboratory undertook the Materials Characterization, Prediction, and Control (MCPC) Laboratory Directed Research and Development Project to advance understanding of nuclear material processing and enable multifold acceleration in the development and qualification of new material systems in national security and advanced energy applications (Smith 2021). The MCPC Project executed research across three scientific vertices—material characterization, predictive modeling, and data analytics—with extensive support by a data curation and management team.

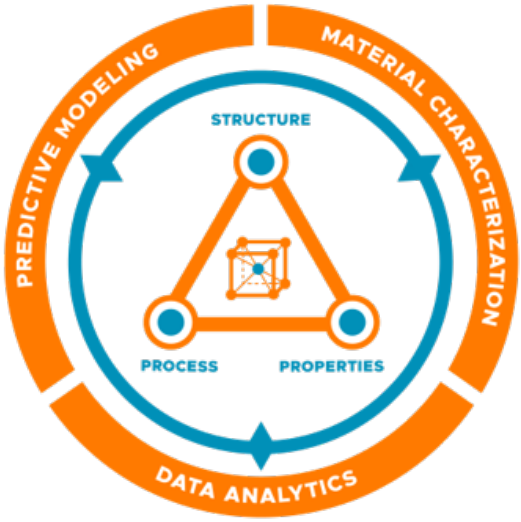

MCPC Project Logo

The central technical objective in the MCPC Project was to improve the prediction and characterization of the process-structure-property relationships within the microstructurally refined region of stainless-steel samples prepared utilizing friction stir processing (FSP). The Material Characterization Vertex within the MCPC Project was tasked with delivering results from two primary characterization approaches: 1) destructive characterization modalities utilizing traditional forms of microstructure and property evaluation, and 2) a nondestructive modality capable of full-volume interrogation for defects and microstructure characteristics. A motivation of the MCPC Project was to demonstrate ultrasonic testing as a nondestructive evaluation (NDE) method to complement traditional destructive methods for characterizing material microstructure, including the potential for real-time inline monitoring.

1.1 Background on Ultrasonic Nondestructive Evaluation

The ultrasonic NDE technique has the potential to be used for real-time inline process monitoring. The technique can be used to detect defects in materials and to characterize material microstructure. Ultrasonic NDE defect detection is well-established, and there are numerous industrial standards and specifications governing how it shall be conducted in the field. Ultrasonic attenuation and backscattering have been used in previous studies to infer material microstructure, such as grain sizes in polycrystalline metals, formed using traditional manufacturing methods. This work establishes an ultrasonic technique for characterizing material microstructure with ultrafine grains that are often produced by FSP.

A grain is a single crystal that is anisotropic in terms of speed of sound. If two neighboring grains are oriented differently, the speed of sound in the direction of propagation will change at the boundary of the two grains, and ultrasonic scattering will happen at the boundary. Scattering causes ultrasonic attenuation and backscatter that are affected by grain sizes and shapes, among other microstructural properties. Grain sizes influence mechanical properties such as yield and tensile strength.

There is high interest in measuring material grain sizes to control material properties during processing or to monitor the change of these properties during service. Traditionally, grain sizes

are measured by optical methods, which are destructive and can be time consuming. As noted earlier, one motivation for the MCPC Project was to establish a capability that can determine grain sizes nondestructively and quickly, which is suitable for in situ use.

Although defect detection was not the main objective of the MCPC Project, a brief demonstration of the capability of ultrasonic NDE is given for materials used in this work.

1.2 Objective

The objective of the work described in this report is to establish a process and an analysis method for measuring grain sizes of stainless steel or other cubic polycrystalline metals with ultrafine grains (grains of 10 microns or less are studied in the present work) using ultrasonic shear wave backscattering based on some prior studies. The work involves five tasks:

1. Measure ultrasonic backscattering experimentally for a series of 316L stainless steel specimens with various grain sizes produced using a friction stir process.
2. Calculate ultrasonic backscattering coefficients from experimental data based on the physical measurement model.
3. Measure ground truth grain sizes of the specimens from Electron Backscatter Diffraction (EBSD) grain boundary images using a generalization of the ASTM E112 intercept method.
4. Build a curve of ultrasonic backscattering coefficients versus the ground truth intercept-based grain sizes to determine the correlation between mean grain sizes and ultrasonic measurements.
5. Demonstrate the ability of using the correlation curve to deduce grain sizes with measured ultrasonic backscattering coefficients for a few 316L stainless steel specimens whose grain sizes were unknown beforehand but were targeted to be an extrapolation to larger grain sizes than those used to formulate the correlation curves.

Experimental procedures and computational algorithms are developed and validated for these tasks as described in Sections 2.0 to 4.0 for a set of FSP experiments. The experiments produced eleven distinct processing conditions with up to three replicate specimens at each processing condition. Subsequently, a set of four additional FSP experiments were undertaken and collectively called the End-to-End (E2E) demonstration. This set used conditions intended to yield distinctly different microstructure from the earlier FSP experiments. Results from these conditions are described in Section 5.0 and show the validity of the developed method to extrapolate to other conditions.

2.0 Specimens and Ultrasonic System for Experiments

To fulfill the objective of measuring grain sizes with ultrasound, backscattering of the material of interest was measured experimentally. The target materials are those made by FSP, and stainless steel of type 316L is of particular interest. Stainless steel is a cubic crystalline material. The techniques developed in this work are generally applicable to cubic crystalline materials with equiaxed grains and with weak or no texture, i.e., the crystallograhic orientations of the materials are close to be random or are fully random and the grains don't have a preferred orientation.

2.1 Stainless Steel of Type 316L Specimens

Stainless steel of type 316L specimens were prepared by FSP experiments under 11 different process conditions that produced specimens with different microstructure characteristics. Table 1 lists the eleven FSP process conditions, each of which includes sensed tool temperature, FSP tool traverse velocity, and tool forge force. Selection of processing conditions was based on subject matter expertise with a desire to produce a range of microstructure and weld qualities (including flaws in the welds in some cases). A total of three distinct FSP experiments were attempted at each condition with the intent of producing three replicate specimens. However, some of these conditions resulted in tool breakage, so replicate specimens were not produced for all conditions.

Table 1. Nominal process parameters of FSP experiments.

Condition ID	Temperature (°C)	Tool Traverse (in/min)	Tool Traverse (mm/min)	Force (lbs)	Force (kN)
C00	N/A	N/A	N/A	N/A	N/A
C01	720	0.5	12.7	9000	40.0
C02	720	0.5	12.7	10500	46.7
C03	720	1.0	25.4	10500	46.7
C04	720	1.0	25.4	9000	40.0
C05	720	3.0	76.2	10500	46.7
C06	750	1.0	25.4	10500	46.7
C07	750	3.0	76.2	10500	46.7
C08	800	1.0	25.4	10500	46.7
C09	800	3.0	76.2	10500	46.7
C10	850	1.0	25.4	10500	46.7
C11	850	3.0	76.2	10500	46.7

Condition ID "C00" represents the unprocessed starting material in the form of a control sample.
"Temperature" is the sensed value within the FSP tool and not the working temperature at the tool/steel interface.

Specimens were prepared from the FSP experiments at each condition, with example specimens shown in Figure 1. Each specimen was marked with a unique *Specimen ID*, and this was MCPC0073 for the NDE specimen shown in the figure. Other specimens are similarly marked with their unique ID.[1] Resulting specimens were characterized in three material characterization "rounds." The correspondence between Specimen ID, Condition ID, and round is provided at the end of this section.

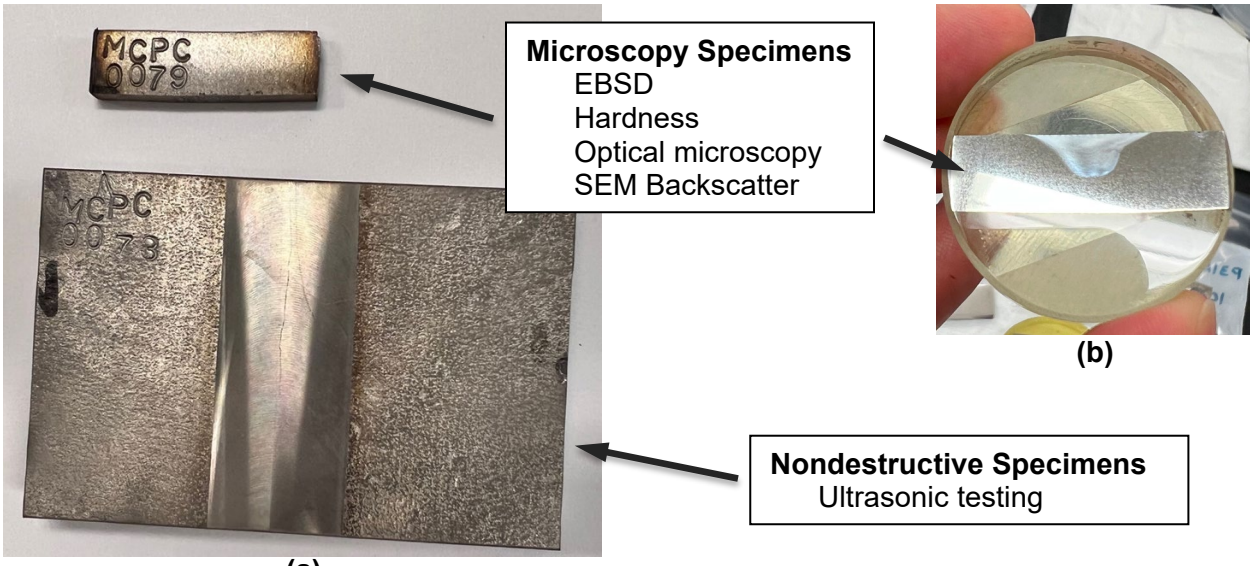

Figure 1. Example FSP specimens.

A NDE specimen was obtained for each nominal processing condition for ultrasonic scanning to study microstructure and its relationships to ultrasonic backscattering.[2] Other specimens were cut next to the NDE specimen for destructive analyses such as optical spectroscopy, SEM, EBSD, and microhardness, as shown in Figure 1. For ground truth grain size measurements, grain boundary images were generated from EBSD images. An example grain boundary image is given in Figure 2.

[1] The top surface of NDE specimens required light machining and sanding to smooth the surface for reliable penetration of the ultrasonic signal. The resulting specimens had a polished finish that is not present in Figure 1. The Specimen ID was reapplied after surface treatment.

[2] Specimens were cut out of large steel parts to support NDE and microscopy characterization efforts within the described experimental program. With the exception of the light surface modification noted earlier, the NDE characterization can be performed without cutting the specimens.

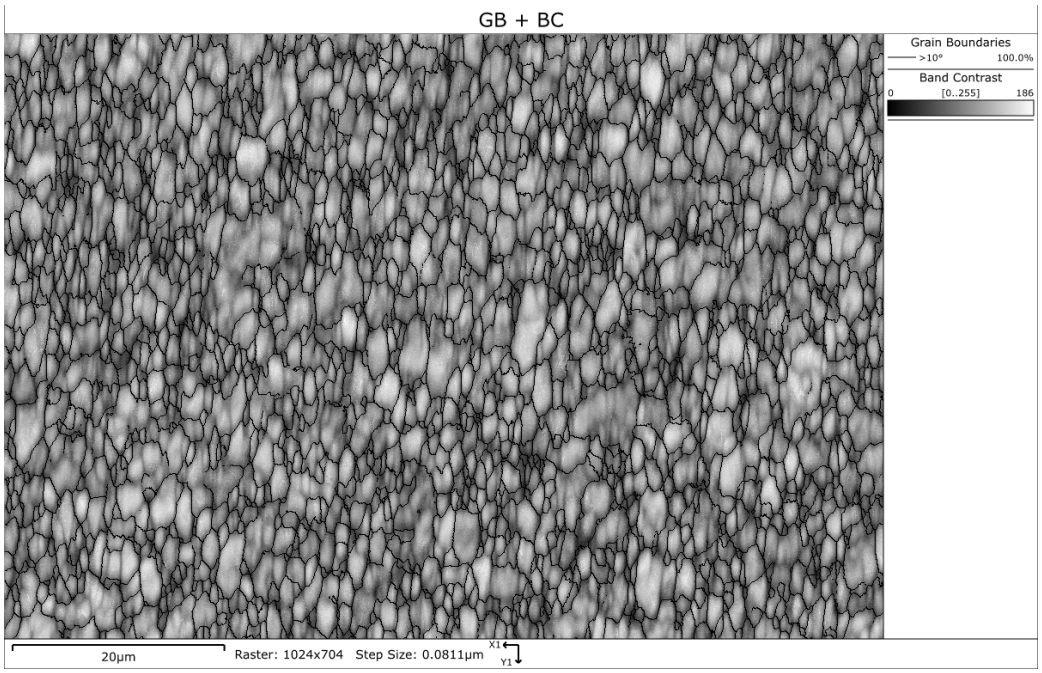

Figure 2. Example of grain boundary image.

EBSD-obtained grain boundary images were analyzed to determine the mean grain sizes using an image analysis method equivalent to that described in ASTM standard E112, Section 13, "Heyn Lineal Intercept Procedure." Specifically, it uses a generalization of the intercept method applied to grain boundary images.[3] The mean grain sizes were measured in terms of the two-point correlation function $P(s)$, the probability that two points, separated by a distance s, are in the same grain. $P(s)$ is generally close to an exponential function of the form $P(s) = e^{-s/b}$ (Stanke et al. 1984). The probability doesn't change across the image, i.e., it is assumed that the grain size distribution stays the same across the image. This is a reasonable assumption since the image covers only a very small surface area about 0.1 mm by 0.1 mm. The parameter, b, with dimensions of length, is the correlation distance, equal to one-half the effective average linear dimensions of the grains and serves as an estimate of the mean grain radius. It is a measure of the mean length of line segments passing through one grain with their end points on grain boundaries. The grain boundary images were analyzed to find mean grain radii by a MATLAB (R2020b) computer program developed at Pacific Northwest National Laboratory. The MATLAB program works as follows in principle.

1. A line of length x is placed in the image, starting from the very top row of the image, with the left end of the line being at the left edge of the image. Set the variable *num* to 1, which is the total number of placements of the line on the image.
2. Determine if the line is within the same grain by checking to see if the line crosses a grain boundary. If the line is within the same grain, set the variable W to 1, otherwise set W to 0. W is the number of times the line is within the same grain.

[3] This "intercept" based method interprets EBSD grain boundary imagery consistent with how ultrasonic signals interact with the grains.

3. If the right end of the line is on the right edge of the image, place the line at the beginning of the next row of the image, with the left end of the line being at the left edge of the image. Otherwise, move the line one pixel to the right. Add 1 to num (*num* = *num* + 1 in programming language).
4. Determine if the line is within the same grain by checking to see if the line crosses a grain boundary. If the line is within the same grain, add 1 to the variable *W* (*W* = *W* + 1), otherwise *W* is not changed.
5. Repeat Steps (3) to (4) till the right end of the line reaches the right edge of the image on the last row of the image.
6. Calculate the probability P(x) of a line of length x is in the same grain: *P*(x) = *W* / *num*.
7. Set x to a different value, and repeat Steps (1) to (6) for this x.
8. After a series of x values are run, *P*(x) is a function of x. This function *P*(x) can be fitted to an exponential function of the form $e^{-x/b}$ by minimizing the squared error *E* between them, and

$$E = \sum_{i=1}^{n} \left| P(x_i) - e^{-x_i/b} \right|^2.$$

   The program searches for a *b* value that makes *E* the smallest. The *b* value that gives the minimum *E* is an estimate of the mean grain radius which is an estimate of the mean distance across a grain along a given direction.

The above analysis can be performed in horizontal direction, in vertical direction, and in any other direction in the plane of the image. Figure 3 gives an example of the probability function *P*(x) (the red curve) in horizontal direction for one of the specimens and its exponential fitting exp(-x/1.08) (the blue curve). In this example, *b*, the mean grain radius, is 1.08 micrometers. The grain boundary images for all the specimens were analyzed using the MATLAB program, and the mean grain sizes (diameters) are shown in Table 2 for the associated microscopy Specimen ID. Table 2 also lists the circle equivalent diameters (CED)[4] and the average microhardness near the center of the stir region obtained from a database of curated material characterization results developed elsewhere for proximate specimens (Todd et al. 2024a; Todd et al. 2024b; Todd et al. 2024c).

[4] Circle equivalent diameter (CED) results were reported with EBSD data. The CED is a value for area that is equivalent to the area of a segmented grain obtained by calculating the number of steps or pixels within the grain. This value is generally smaller than an intercept-based grain size.

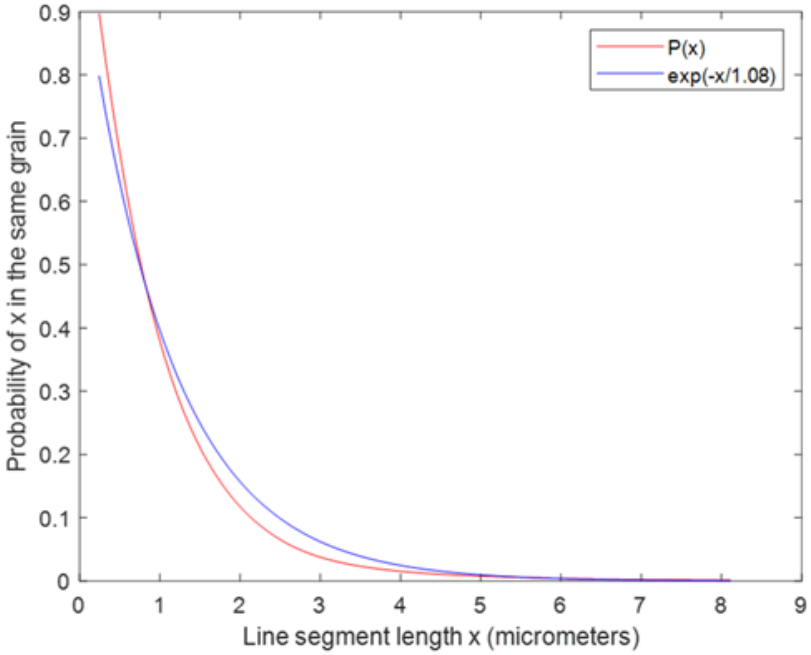

Figure 3. Probability function and its exponential fitting.

As stated earlier, the MATLAB program uses an analysis method equivalent to the intercept method in the ASTM standard E-112. The value *b* calculated by the program is approximately equal to the mean lineal intercept length by the intercept method, as verified by related work to this project, and the detailed description of this work is attached to this report as Appendix A.

Table 2. Mean grain diameter (μm) and hardness of FSP specimens.

	Condition ID	Specimen ID	Gain size (μm)		Hardness
			Intercept	CED	
Round 1	C01	MCPC0153	1.40	1.2	275
	C02	MCPC0138	1.34	N/A	305
	C03	MCPC0003	1.56	1.0	267
	C04	MCPC0158	1.42	1.0	273
	C05	MCPC0008	2.04	1.2	264
	C06	MCPC0013	2.16	1.6	259
	C07	MCPC0018	2.42	1.5	243
	C08	MCPC0023	2.82	2.1	234
	C09	MCPC0028	3.36	2.1	231
	C10	MCPC0033	5.72	3.0	210
	C11	MCPC0038	4.52	2.5	205
Round 2	C01	MCPC0163	1.42	0.80	291
	C02	MCPC0118	1.48	0.80	292
	C03	MCPC0043	1.58	0.90	274
	C04	N/A			
	C05	MCPC0048	1.86	1.17	265
	C06	MCPC0053	1.52	N/A	276
	C07	MCPC0058	1.30	N/A	275
	C08	MCPC0063	4.14	2.02	228
	C09	MCPC0068	3.29	2.33	228
	C10	MCPC0073	4.87	3.12	215
	C11	MCPC0078	4.86	3.25	212
Round 3	C01	MCPC0168	1.04	0.8	289
	C02	N/A			
	C03	MCPC0113	1.38	1.0	283
	C04	N/A			
	C05	N/A			
	C06	MCPC0103	1.92	1.3	261
	C07	MCPC0108	2.50	1.6	249
	C08	MCPC0083	3.94	2.3	229
	C09	MCPC0088	3.04	1.7	233
	C10	MCPC0093	N/A	4.3	228
	C11	MCPC0098	N/A	2.7	218

2.2 Ultrasonic Scanning and Data Acquisition System

To measure ultrasonic backscattering, an Imaginant PureView-La1 ultrasonic pulser and receiver module (S/N JE0111) are used to excite ultrasonic transducers and receive/condition returned signals from the sample. The raw A-scans are subsequently digitized at 500 MHz

sampling frequency and saved to files for later analysis to extract backscattering coefficients. The specimen and the transducer are immersed in a water tank. The transducer is mounted on a 3-axis scanning system and scanned over the sample to acquire A-scans from multiple positions for averaging. The scanning and data acquisition system is shown in Figure 4 below.

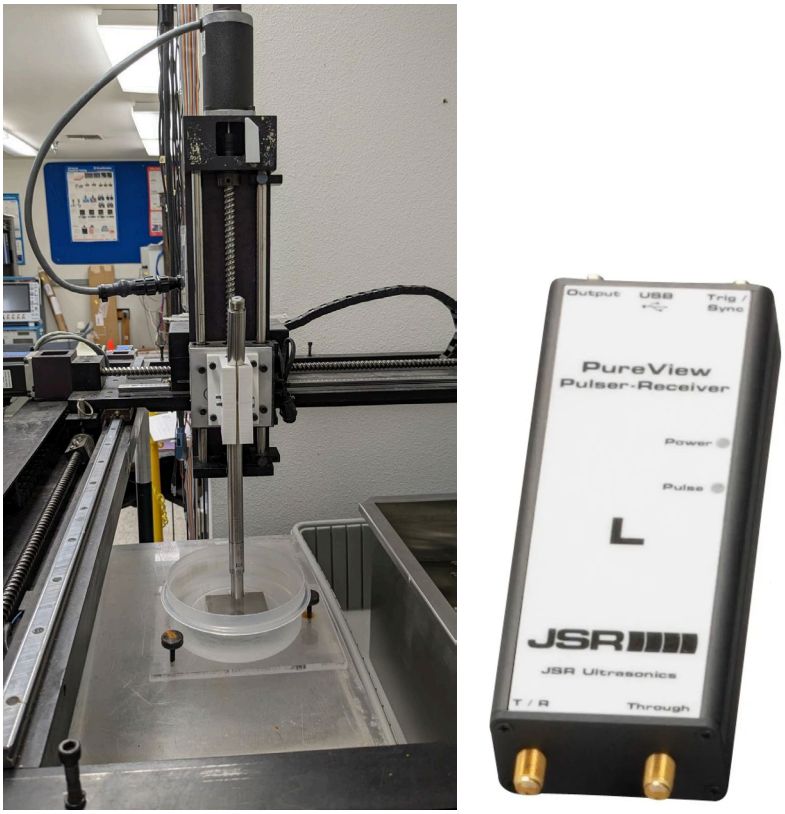

Figure 4. Ultrasonic scanning and data acquisition system.

The PureView-La1 is a miniaturized pulser-receiver at 124 mm × 50 mm × 25 mm, and it is universal serial bus (USB) controlled and USB powered. Table 3 lists its pulser characteristics and its receiver characteristics. Table 4 lists the characteristics of the transducer used for this work.

Table 3. PureView-La1 characteristics.

Pulser Characteristics						
Model	Fall time Maximum (ns)	Pulse Width Typical (ns)	Pulse Amplitude Min (V)	Pulse Energy (µJ)	Maximum PRF (kHz)	Damping (Ohms)
JPV-PR-USB-La1	5 5.5	70 210	-135 -148	61 247	10 2.5	400, 200, 70, 46
Receiver Characteristics						
Model	Modes	Bandwidth (MHz)	Gain (dB)	High Pass Filters (MHz)	Low Pass Filters (MHz)	
JPV-PR-USB-La1	Echo or Through	1-100	-11.5 to 70	1, 12.5	60, 100	

Table 4. Ultrasonic transducer characteristics.

Manufacturer	Model Number	Serial Number	Frequency	Diameter	Focal Length
NDT Systems	BHF202	065120	20 MHz	0.25 in.	1.0 in.

The ultrasonic scanning system can perform XYZ 3-axis scans. For this study, XY raster scans are conducted. The scan direction is normal to the weld line, and the scan resolution is 0.2 mm. The index direction is along the weld line, and the index resolution is 1 mm. The scanner can stop the transducer at each scanning location and let the data acquisition acquire multiple waveforms and perform averaging to reduce random noise, which could be high relative to grain noise.

Both ultrasonic longitudinal wave and shear wave are used in this study. This webpage explains the difference between the longitudinal wave and the shear wave (Olympus 2024). To generate shear waves in the specimen through water coupling in a water bath, a nonzero incident angle is required. A 3-D-printed adaptor was made with a through hole at an angle of 19.6 degrees for the transducer search tube. With this incident angle, a 45-degree shear wave will be generated through mode conversion[5] after the ultrasonic beam transmits into the specimen. The adaptor will guarantee the same incident angle for all specimens for better repeatability. The adaptor also has a through hole for the search tube at zero angle to facilitate generation of longitudinal wave in a specimen and also a reference signal acquisition. A sketch of the adaptor is shown in Figure 5.

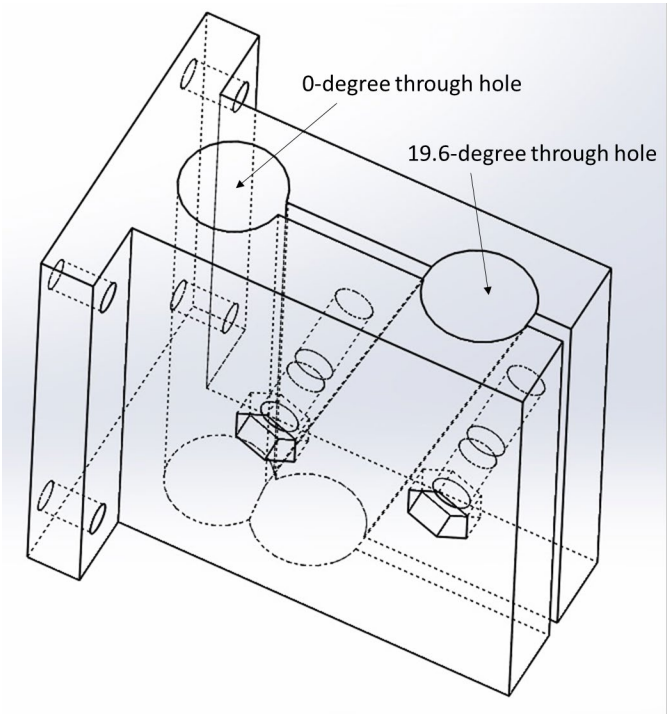

Figure 5. 3-D-printed adaptor for shear wave generation and reference signal acquisition.

[5] Mode conversion occurs when a wave encounters an interface between materials of different acoustic impedances and the incident angle is not normal to the interface. When an ultrasonic wave such as a longitudinal wave in the first material enters the second material, it converts to a different type of wave, such as a shear wave.

3.0 Demonstration of Defect Detection Capability

The friction stir process used to produce the specimens can introduce unwanted defects in the material, such as lack-of-fusion defects and voids/pores. Some conditions in Table 1 were found to introduce defects, such as Condition C05 that was used to produce the NDE specimen MCPC0008 with known defects that were studied in the current section. Ultrasonic longitudinal or shear waves can be used to detect such defects in a pulse/echo configuration, i.e., the same transducer is used to excite ultrasound and receive any energy reflected back to it by a defect. To demonstrate this capability, a specimen with known porosity was scanned with a longitudinal wave. The test configuration is shown in Figure 6. The ultrasonic probe was normal to the specimen so that the incident angle was zero. A longitudinal wave was transmitted into the specimen.

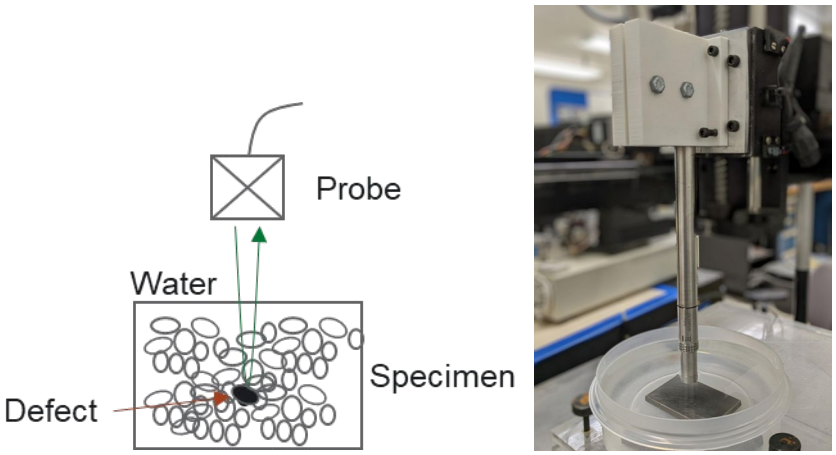

Figure 6. Setup for defect detection.

Figure 7 shows the microscopic image of a specimen adjacent to the NDE specimen MCPC0008. There are defects at the lower right edge of the stir zone (the area encircled by the red dashed line), either lack of fusion or voids. With the setup in Figure 6, a raster scan of 2.0 inches by 2.0 inches was performed with a scan resolution of 0.2 mm and an index resolution of 1.0 mm. The transducer is listed in Table 4. Figure 8 shows the B-scan[6] for one of the transverse cross-sections. In the B-scan, the area with red and yellow bright colors is caused by the defects that reflected strong signals back to the transducer. This example indicates that the ultrasonic method can detect this kind of manufacturing defect. Effort to characterize detected flaws for size or other characteristics is not undertaken in this project.

[6] "B-Scan" is standard terminology in ultrasonic testing for a two-dimensional graphical presentation of data in which the travel time of an ultrasonic pulse is represented as a displacement along one axis, and transducer movement is represented as a displacement along the other axis.

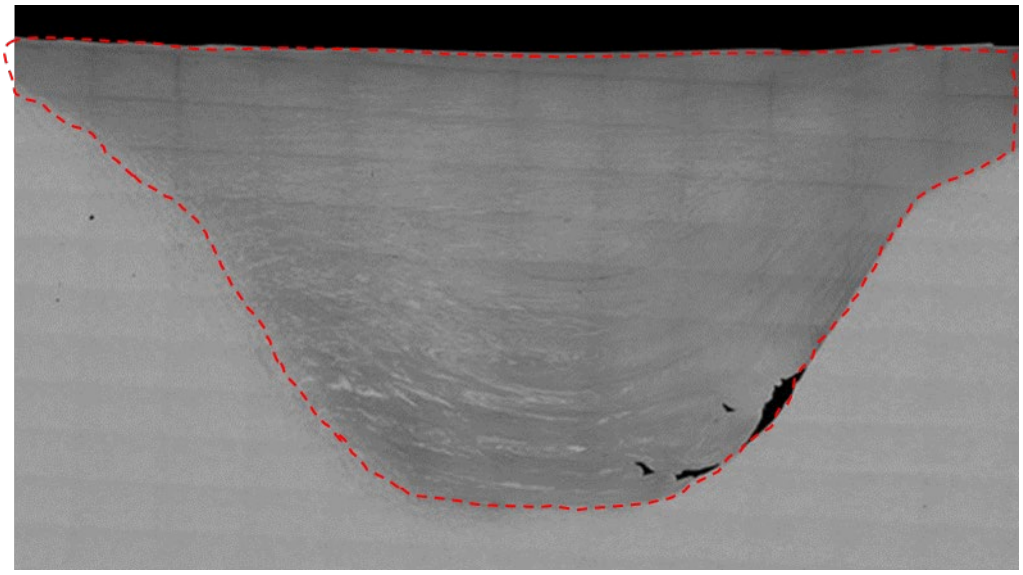

Figure 7. Optical image of a specimen adjacent the NDE specimen MCPC0008 with defects.

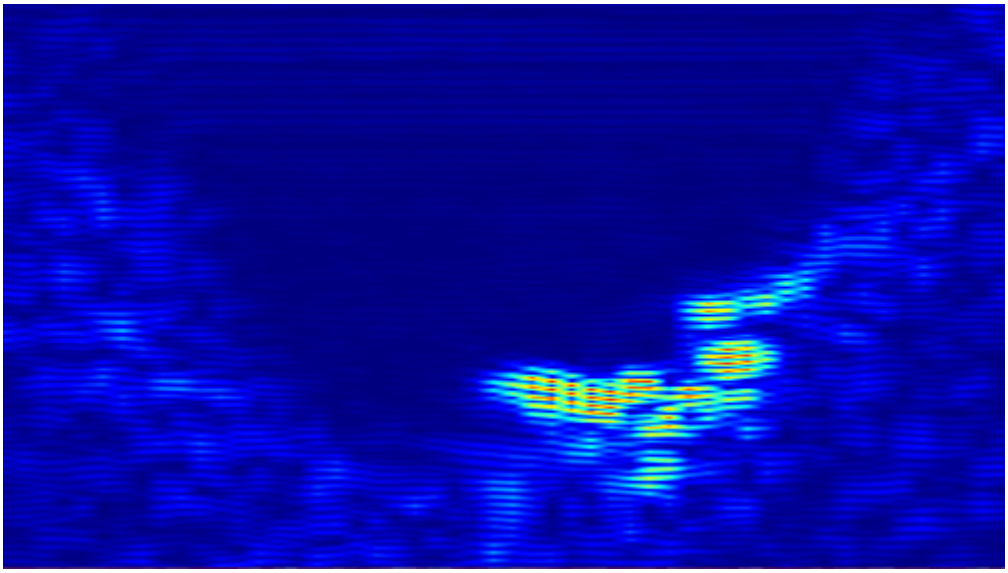

Figure 8. Ultrasonic B-Scan image of the NDE specimen MCPC0008 with defects.

4.0 Measurements of Ultrasonic Backscattering

4.1 Setup and Method

Backscattering was measured by acquiring grain noise waveforms and removing the effects of the measurement system using models. The experimental procedure was developed at the Center for Nondestructive Evaluation at Iowa State University (Margetan et al. 1993b). It involved using a focused transducer to scan over the specimen of interest and gathering a grain noise waveform at each transducer location, as shown schematically in Figure 9. There are two types of ultrasonic waves that can be introduced into the specimen: longitudinal wave and shear wave. Since the speed of sound for a longitudinal wave is close to twice that for a shear wave, at the same frequency, the wavelength of the longitudinal wave is close to twice that of the shear wave. As a result, if the same frequency is used, shear waves generate stronger grain noise signals and a higher signal-to-noise ratio because they have shorter wavelengths and produce more scattering. The specimens in this study have grains in the range of one micron to a few microns. Initial tests showed that for longitudinal waves at 20 MHz, these grains generated weak grain signals and poor signal-to-noise ratio. On the other hand, for shear waves at 20 MHz, these grains generated stronger grain signals with at least 3 to 1 signal-to-noise ratios even for all the specimens studied. Shear waves were therefore chosen to acquire grain noises for all specimens.

Figure 9 shows the ultrasonic transducer is at an angle to the beam entry surface. This means the incident angle is 19.6 degrees. Mode conversion happens for the wave after it transmits through the water/steel interface. By mode conversion, shear waves are introduced in the specimen at a 45-degree angle with respect to the entry surface.

Raster scans of 50 mm by 50 mm are performed. Scan lines are normal to the weld line. Scan steps are 0.2 mm and index steps are 1.0 mm, so each raster scan contains 2550 scan positions and 2550 ultrasonic A-scan waveforms[7]. Each scan position has one A-scan waveform acquired which is the average of 200 waveforms coming from that position.

[7] “A-Scan” is standard terminology in ultrasonic testing in which the received pulse amplitude is represented as a displacement along one axis (usually the y-axis) and the travel time of the ultrasonic pulse is represented as a displacement along the other axis (usually the x-axis).

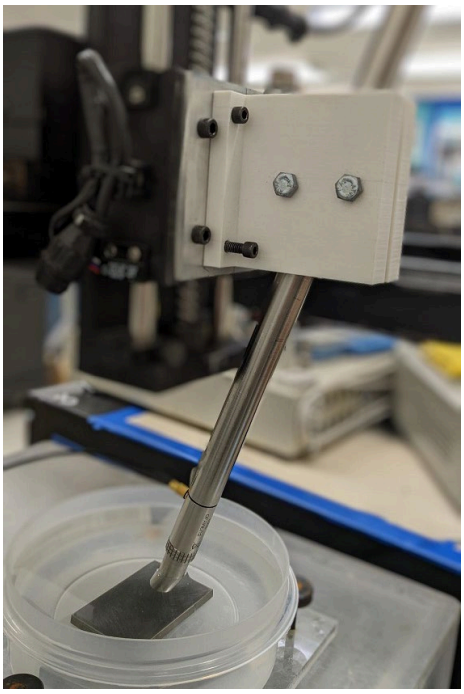

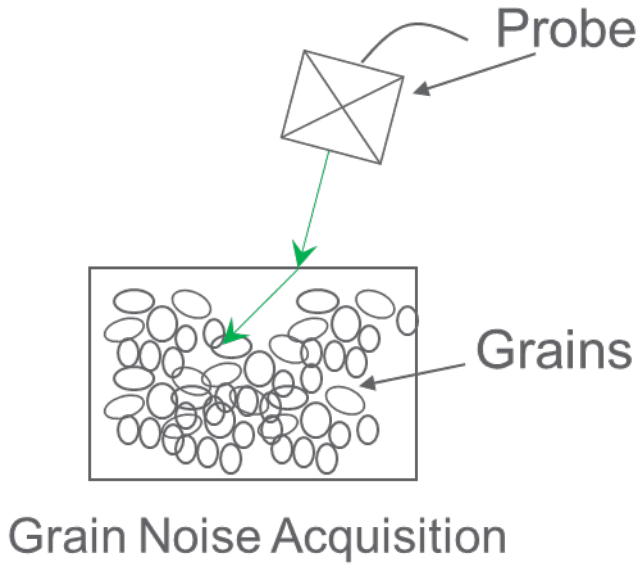

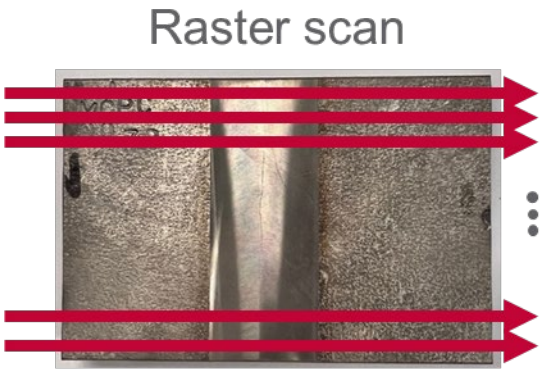

Figure 9. Setup for backscattering measurements.

Figure 10 shows typical A-scan waveforms of the grain noise through the base material only (a) and through the stir zone (b) for the specimen MCPC0158. The beam entry surface is at 24 μs or 17.8 mm from the transducer face, and knowing the sound speed of the material, the distance from the surface can be determined from time after surface entry. The base material has relatively large grains with diameters around 40 microns, but in the stir zone the grains are only a few microns in diameter. Figure 10(a) shows that large grains generate higher grain noise as expected. Figure 10(b) shows that grain noise is low in the stir zone and after the stir zone grain noise is high because the sound goes from small grains to large grains as it goes across the stir zone boundary into the base material just below the stir zone.

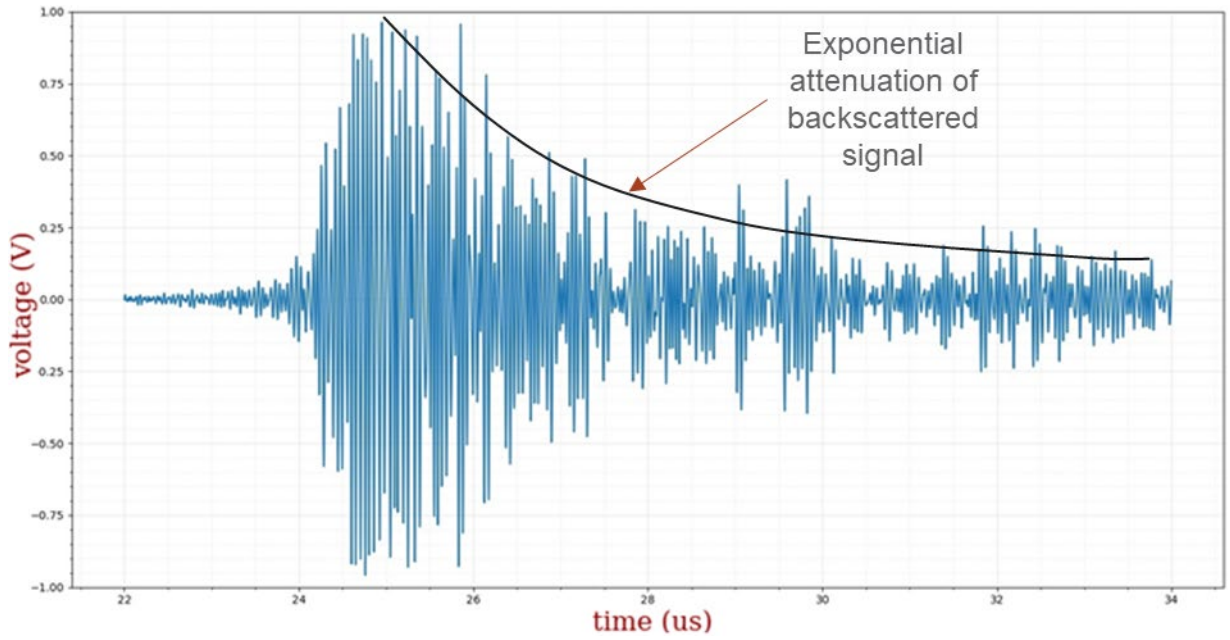

(a) Grain Noise in the Base Material

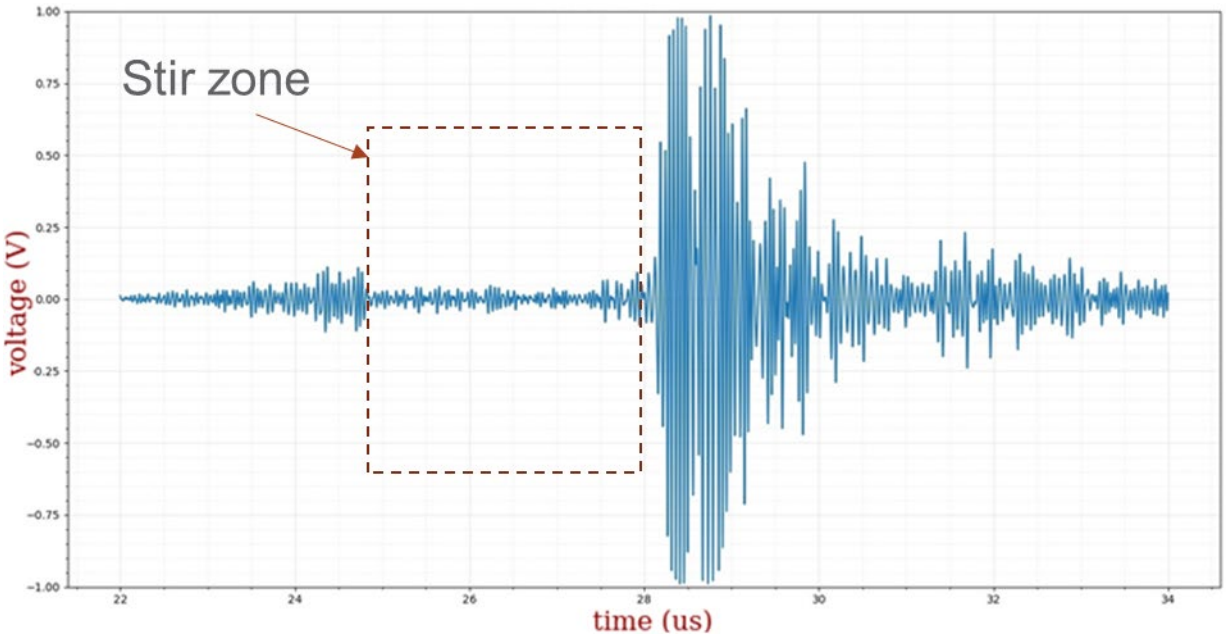

(b) Grain Noise in the Stir Zone

Figure 10. Typical A-scan waveforms of grain noise.

Figure 11 shows a typical ultrasonic B-scan of the transverse cross section of the specimen. It consists of all the A-scan waveforms in one scan line, with each vertical line of the image being a waveform. The grain noise signature in the stir zone is clearly different from that of the base material, as the stir zone grains generate much weaker grain noise.

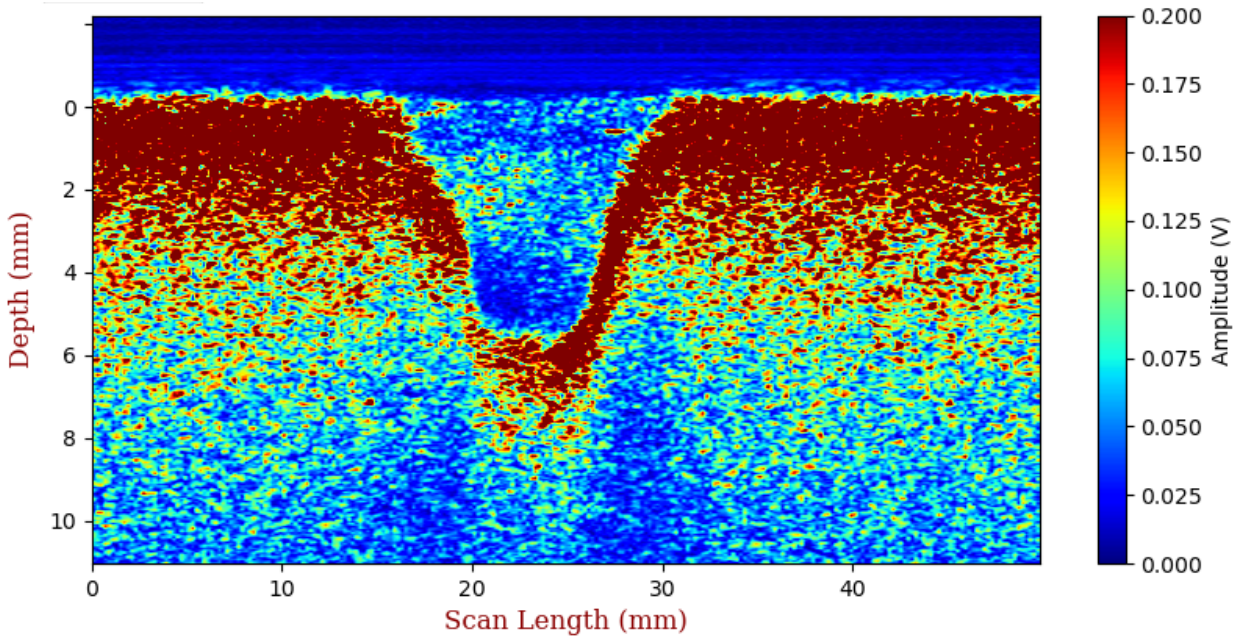

Figure 11. Typical B-scan of grain noise.

To analyze the acquired waveforms and derive backscattering coefficients that are related exclusively to material property and microstructure yet independent of the measurement system, it is necessary to remove the effects of the measurement system and a particular measurement configuration, such as pulser and receiver settings, probe characteristics, water path, incident angle, etc.. This is accomplished by models of the backscattering measurement that assume that the noise signal is an incoherent sum of the signals scattered by individual grains (Margetan et al. 1991; Margetan et al. 1992). The measured grain noise waveform includes contributions from a collection of grains. The root-mean-squared (rms) noise, $\Gamma_{\text{rms}}(\omega)$, is used to describe the total noise magnitude in the frequency domain. Γ_{rms} is defined as

$$\Gamma_{rms}(\omega) = \sqrt{< |\Gamma_{noise}(\omega)|^2 >}; t_a \le t \le t_b \qquad 4.1$$

where $\Gamma_{noise}(\omega)$ denotes the Fourier component of the measured noise signal at a transducer location at angular frequency ω on the finite time interval indicated above. <> denotes the average over many transducer scanning positions (or grain ensembles). The time domain echoes within the time interval are regarded as resulting from the backscattering of sound by all grains located in a corresponding volume R of the specimen. Γ_{rms} is related to the microstructure and the measurement geometry (Margetan et al. 1993a)

$$\Gamma_{rms}(\omega) = \beta(\omega)\sqrt{n}A_{rms}(\omega)\left[\frac{2T_{01}^2\rho_1 v_1\, exp(-2\alpha_0 z_{0s})}{k_1 a_x a_y \rho_0 v_0}\right]\left[\iiint_R |C(\omega)|^4\, exp(-4\alpha_1 z_1)\, dx_1 dy_1 dz_1\right]^{1/2}; \left(\frac{t_a v_1}{2} \le z_1 \le \frac{t_b v_1}{2}\right). \qquad 4.2$$

n: the number of grains per unit volume;

A_{rms}: the root-mean-square average far-field scattering amplitude of a single grain; subscripts 0 and 1 refer to water and metal, respectively;

z_{0s}: the inspection water path;

T_{01}: the plane wave transmission coefficient at the water/solid interface;
$C(\omega)$: accounts for beam diffraction and describes the incident ultrasonic displacement field in the metal;
ρ_0: density of water;
ρ_1: density of metal;
v_0: longitudinal wave speed in water;
v_1: longitudinal wave speed in metal;
α_0: ultrasonic attenuation coefficient in water;
α_1: ultrasonic attenuation coefficient in metal;
k_1: ultrasonic wave number in metal;
a_x and a_y: the radii of the elliptical piezoelectric element of the transducer in the two lateral directions, $a_x = a_y$ for circular element.

The frequency-dependent product $n^{1/2}A_{rms}(\omega)$ is defined to be the specimen's "Figure-of-Merit" (FOM), which is a measure of the noise-generating capacity of the microstructure. The FOM is equal to the square root of the widely used grain-noise backscattering coefficient η (Gubernatis et al. 1977). The transducer efficiency factor $\beta(\omega)$ can be obtained from a reference measurement, for example, a front surface echo from the specimen itself. The FOM can be deduced from Equation (4.2) by experimentally determining $\Gamma_{\text{rms}}(\omega)$ and then using models (Margetan et al. 1993b) of the measurement process to remove the influence of the other factors.

As an example, Figure 12 shows the $\Gamma_{\text{rms}}(\omega)$ results for a set of scans collected for the processing conditions indicated in Table 2 and associated with the "Round 1" material characterization effort. Results in this figure indicated as MCPC0033-2 and MCPC0158-2 are replicate ultrasonic testing (UT) scans of MCPC0033 and MCPC0158, respectively. These results are for the stir zone only except for the specimen MCPC0178 which was not processed by FSP and contains base material only as a reference. Based on the grain size data in Table 2, the basic trend in Figure 12 is that the larger the grain size, the stronger the $\Gamma_{\text{rms}}(\omega)$. MCPC0178 has the strongest the $\Gamma_{\text{rms}}(\omega)$ since it has much larger mean grain size at around 40 microns.

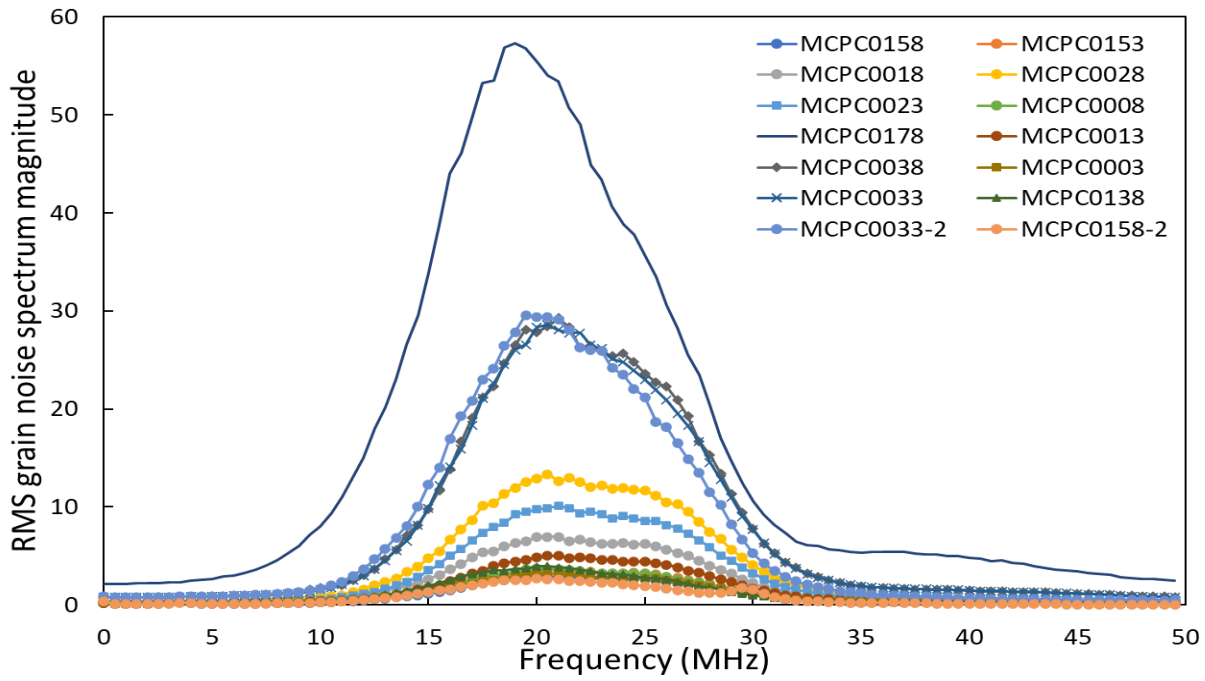

Figure 12. The rms noise $\Gamma_{\text{rms}}(\omega)$ for Round 1 specimens.

Figure 13 shows the setup for the reference signal acquisition. The ultrasonic beam is normal to the surface of the specimen. The reference signal is the echo from the water/metal interface. For a focused transducer, if the water path, Z_{0R}, is set to be equal to its focal length F, then the spectrum of the reference signal $\Gamma_{ref}(\omega)$ is given by

$$\Gamma_{ref}(\omega) = \beta(\omega) R_{00} D(\omega) e^{-2jk_0 z_{0R}} e^{-2\alpha_0 z_{0R}} \tag{4.3}$$

with

$$R_{00} = \frac{\rho_0 v_0 - \rho_1 v_1}{\rho_0 v_0 + \rho_1 v_1} \tag{4.4}$$

and

$$D(\omega) = 1 - e^{-\frac{j2\pi}{S}}\left[J_0\left(\frac{2\pi}{S}\right) + jJ_1\left(\frac{2\pi}{S}\right)\right]; \quad S = \frac{4\pi v_0 z_{0R}}{\omega a^2} \tag{4.5}$$

Here J_m denotes the ordinary Bessel function of integral order m, and the factor D accounts for the effects of beam diffraction and focusing.

Figure 14 shows an example reference signal, which is the echo from the front surface of the specimen.

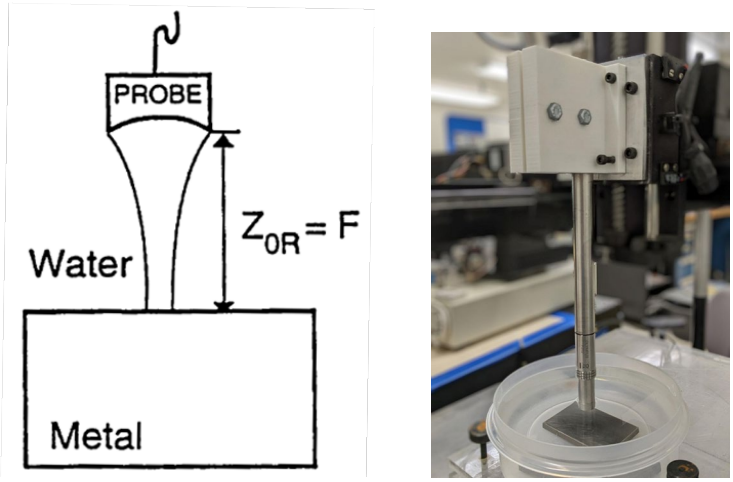

Figure 13. Setup for reference signal acquisition.

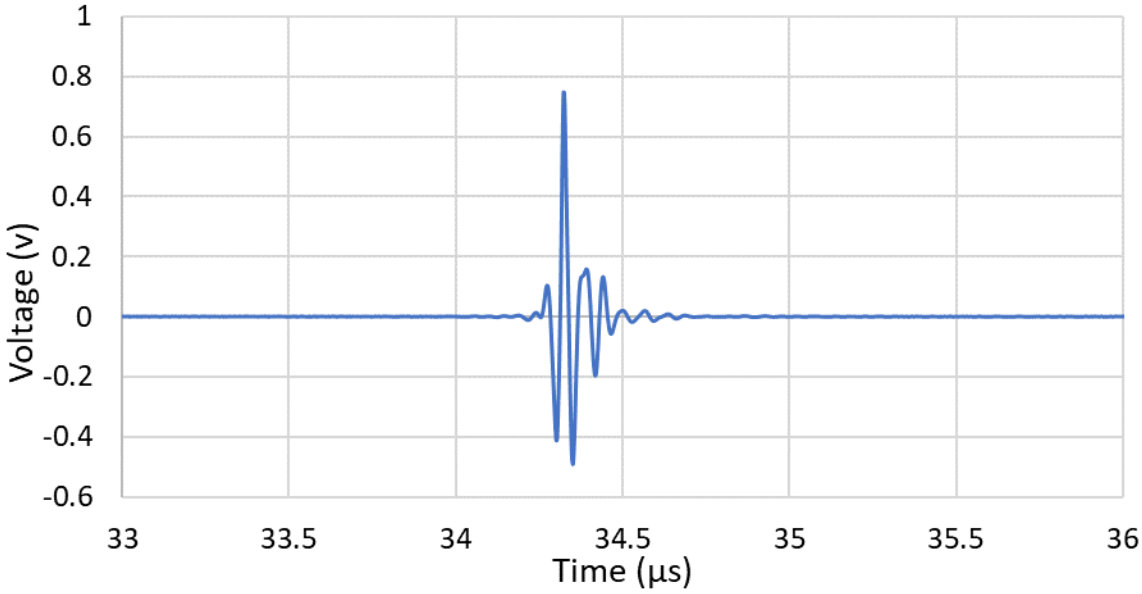

Figure 14. Example reference signal.

The transducer used to measure FOM for the specimens is listed in Table 4. Two acquisitions will be made: first, acquisition of a reference signal from the front surface of the sample with just one A-Scan waveform; second, acquisition of grain noise signals. For the acquisition of the reference signal, the water path must be equal to the focal length of the transducer. For the grain noise acquisitions, the water paths are chosen so that the sound beam focuses 3 mm below the front surface of each sample. An area of 50 (normal to the weld line) × 50 (along the weld line) millimeters of the specimen around the center will be scanned in 0.2 mm increments normal to the weld line and in 1.0 mm increments along the weld line. Raw A-Scan waveforms will be acquired. The general procedure is given below:

1. Turn on the motion control box if not already on. Start the MotionGUI program. Click the “Connect to ACR” button and then the “Initialize ACR” button if not already connected and initialized. Make sure the motion axes are working.

2. Set the time delay of the DG535 delay box to 32 microseconds.
3. Set the oscilloscope TBase to 34.3 μs, the horizontal scale to 2 μs/div., and the vertical scale to 500 mV/div.
4. On the MotionGUI program, click the “Scope Settings” button. Click “Initialize” if not already initialized. Set the Gage card scope settings to start at 0 and stop at 5 microseconds, range at +/- 1V, and sampling frequency at 500 MHz. If any changes are made, click “Update Settings.”
5. Connect the PureView-L Pulser/Receiver module to a USB port of the computer if not already connected. Start JSR .NET Control Panel program. Set “Receiver Mode” to Echo. Set Gain to 20 dB. Set Low Pass Filter to 60 MHz and High Pass Filter to 12.5 MHz. Check “Trigger Enable.” Set Trigger Source to External. Check “Pulser Voltage Supply Enable.” Set Damping to 400 ohms. Set Trigger Input Impedance to 50 ohms.
6. Place the sample in the water tank with its label in the upper left corner and its arrow pointing toward the -X direction and the polished face up.
7. Align the long edge of the sample with the Y axis.
8. Set the transducer incident angle to be zero, i.e., connect to the search tube at a zero angle. Make sure the label on the transducer faces the +X direction.
9. Center the transducer over the sample by eyeballing.
10. Set the water path to 1 inch roughly by adjusting the water path so that the front surface echo is at 34 μs. The fractional shortening (FS) echo should be entirely visible on the Gage card scope screen and on the oscilloscope, and no other echoes are visible before it.
11. Remove any air bubbles on the sample top surface and on the face of the transducer.
12. Level the sample by moving the probe in X and Y directions across the sample surface till the time of flight of the FS echo does not change more than 200 nanoseconds. (Tip: Set the oscilloscope horizontal scale to 100 ns/div for easier viewing of the movement. Set it back to 2 μs/div after this step is finished.)
13. Adjust the water path so that the center of the front surface echo is at 34.3 μs (to make a 1 inch water path).
14. Center the transducer over the sample by eyeballing
15. Adjust the gain of the UT receiver so that the FS echo is between 1.2 and 1.6 Vpp.
16. Set the motion scan axis to be Y and the index axis to be X. Set X Step Size to 1 mm and X Distance to 1 mm. Set Y Step Size to 1 mm and Y Distance to 1 mm.
17. On the MotionGUI program, uncheck “Manual Sync,” choose a file (MCPCxxxx_yyyy_FS.csv, where xxxx is the specimen number and yyyy is a sequential scan number), check “Record Data”, and check “Provide Sync.”
18. Activate “Average” function by checking “Settle” and setting to do 200 averages and set the rep rate to 200. Set scan speed to 25 mm/s. Start the scan.
19. When the scan is finished, click “Close File,” uncheck “Provide Sync,” uncheck “Settle,” and check “Manual Sync.”
20. Change the transducer angle to 19.5 degrees in the XZ plane toward the -X direction by moving the transducer to the search tube at that angle. Make sure the label on the transducer faces the +X direction.

21. Set oscilloscope TBase to 24 μs, horizontal scale to 2 μs/div., vertical scale to 500 mv/div.
22. Adjust the water path so that the beginning of the front surface echo is at 24 μs. This will make the beam focus at 2.5 mm below the front surface. Make sure you are not working on the wrong signal. (There should not be any signal between the initial pulse and the front surface echo.)
23. Center the transducer over the sample in Y direction by finding the two edges of the sample by drop of the FS echo.
24. Set the time delay of the DG535 delay box to 22 microseconds. Set the Gage card scope settings to start at 0 and stop at 12 microseconds, Range at +/- 1V, Sampling frequency at 500 MHz. Click “Update Settings.” The FS echo and subsequent grain noise should be entirely visible on the Gage card scope screen and on the oscilloscope.
25. Adjust the gain of the UT receiver so that the grain noise signals after the FS echo are maximized, but take care to make sure they will never saturate during scanning. Normally the gain should be at 70 dB.
26. Set the motion scan axis to be Y and the index axis to be X. Set X Step Size to 1 mm and X Distance to 50 mm. Set Y Step Size to 0.2 mm and Y Distance to 50 mm.
27. The scan area will be 50 mm by 50 mm. Move the probe in the X direction to find the edge, which will be the scan starting point for X. Move the probe to the scan starting position in Y, which is -25 mm from the center position in both Y directions.
28. On the MotionGUI program, uncheck “Manual Sync,” choose a file (MCPCxxxx_yyyy_GN.csv), check “Record Data,” and check “Provide Sync.”
29. Activate “Average” function by checking “Settle” and setting to do 200 averages and set the rep rate to 200. Set scan speed to 25 mm/s. Start the scan.
30. When the scan is finished, click “Close File,” uncheck “Provide Sync,” uncheck “Settle,” and check “Manual Sync.”

4.2 Results

Data were acquired for 29 specimens indicated in Table 2. For each specimen the scan and data acquisition took about four hours to complete. Most of the time was due to stoppage at each scan position for acquiring and averaging 200 waveforms to reduce excessive unwanted electronic noise. To speed up testing and reduce scanning time in in situ applications, it is necessary to use an UT system with low electronic noise that doesn’t need averaging and stoppage at each scan position.

A FORTRAN 90 program based on Equations (4.1), (4.2), and (4.3) were used to calculate FOM from the acquired A-scans.

To calculate FOM, only the data inside the stir zone was used. A time gate is also used to limit data in a depth range that is the distance the sound travels within the time in the gate. For the following FOM results, the center of the time gate is two microseconds below the front surface, and its length is 1.024 microseconds, or 512 data samples. Figure 15 shows the approximate location where the bounding box for data analysis is located. The bounding box is chosen to avoid interference both from the top surface and from the transition area of the stir zone.

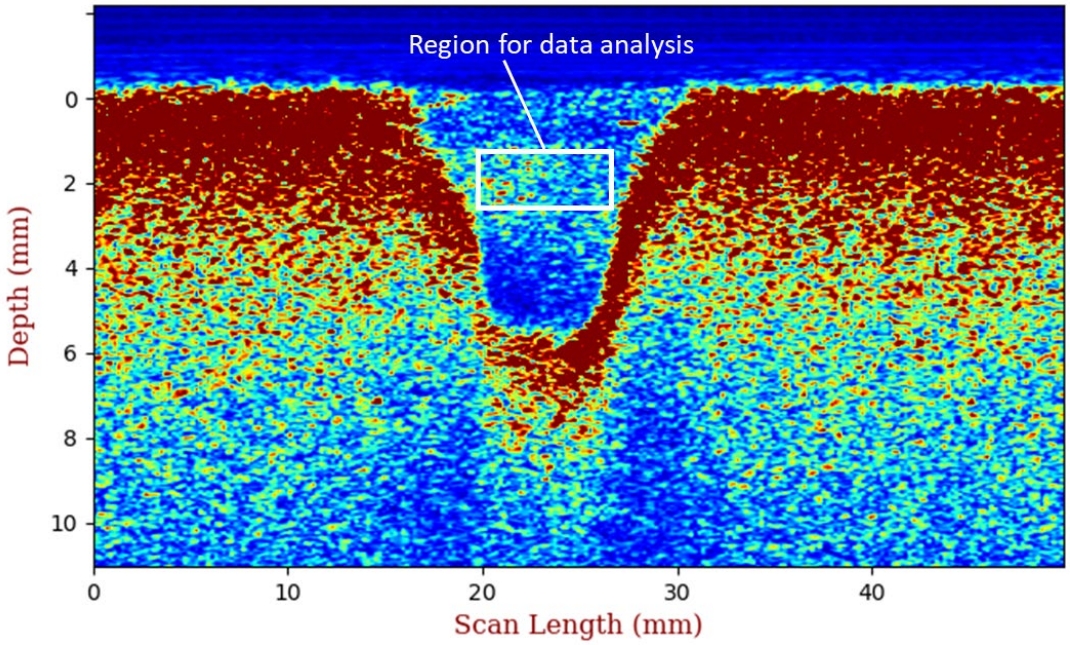

Figure 15. Region for data analysis.

Figure 16 presents the results of the FOM measurements versus grain sizes in diameters based on the intercept method. Note that the FOM vs. Mean Grain Size plot does not include the Round 3 C10 specimen and C11 specimen data points because their grain boundary images do not have 50 grains in any direction, falling short of the requirement of ASTM E112 Standard for the intercept-based grain size measurement.

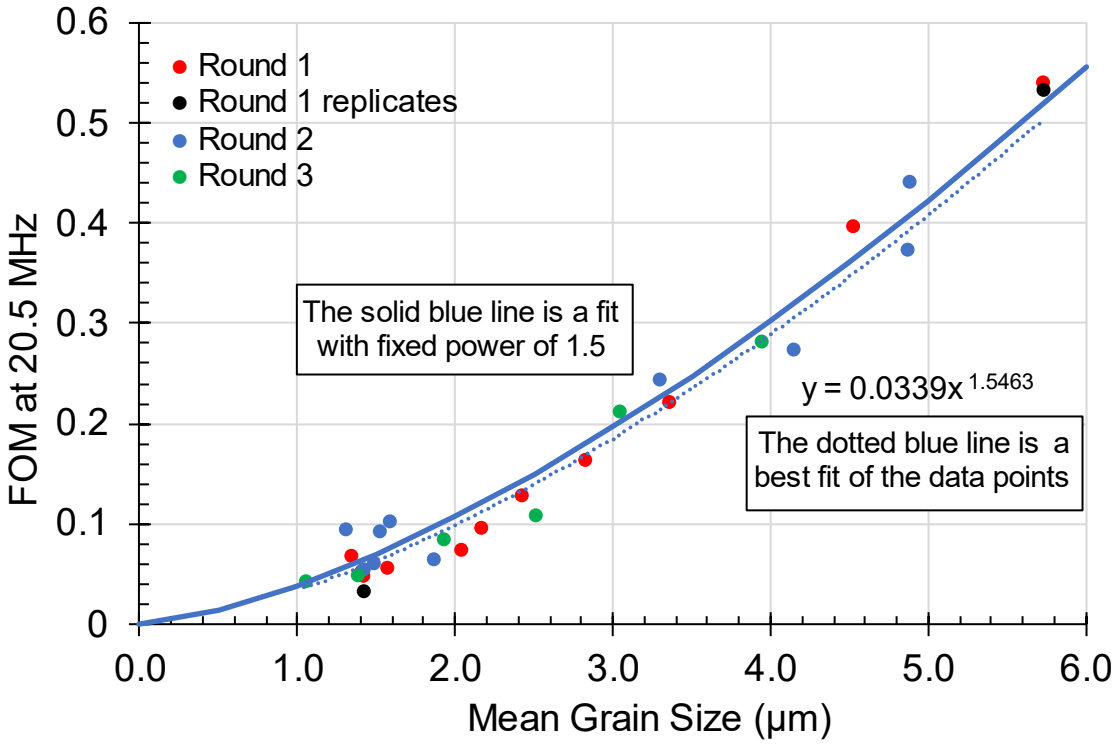

Figure 16. Measured backscattering (FOM) vs. grain sizes (from intercept method).

The results of FOMs versus grain sizes show a strong correlation between the ultrasonic backscattering measurements and grain sizes, even for small grains at just a few micrometers in diameter. The correlation coefficient between the measurement points in the plot and the solid blue fit curve is 0.988, meaning the correlation is very strong. This makes it possible to measure grain sizes of ultrafine grains from ultrasonic backscattering measurements.

The data in Figure 16 can be fitted into a trendline with a power of roughly 1.5. This is consistent with ultrasonic backscattering theories for cubic polycrystalline materials that show the FOM is proportional to the grain diameter raised to the power of 1.5 (Rose 1991,1992,1993 QNDE; Ahmed et al. 1995 QNDE; Guo et al. 2003 QNDE), as shown in the following formula, where *C* is a constant for a specific material, $\bar{D}$ is the mean grain diameter from the intercept method, and *f* is the frequency.

$$FOM = C\bar{D}^{1.5}f^2$$

In Figure 16 the solid blue line has the following formula.

$$FOM = 0.0378\bar{D}^{1.5}$$

Table tabulates all the FOM data for all three rounds, together with grain sizes based on the intercept method, grain sizes based on the CED method, and hardness measurements.

Table 5. FOM and mean grain diameter of FSP specimens.

	Condition ID	Specimen ID	Gain size (μm) Intercept	Gain size (μm) CED	FOM @ 20.5 MHz	Hardness
Round 1	C01	MCPC0153	1.40	1.20	0.0519	275
	C02	MCPC0138	1.34	N/A	0.0671	305
	C03	MCPC0003	1.56	1.00	0.0552	267
	C04	MCPC0158	1.42	1.00	0.0471	273
	C05	MCPC0008	2.04	1.20	0.0730	264
	C06	MCPC0013	2.16	1.60	0.0964	259
	C07	MCPC0018	2.42	1.50	0.1292	243
	C08	MCPC0023	2.82	2.10	0.1634	234
	C09	MCPC0028	3.36	2.10	0.2211	231
	C10	MCPC0033	5.72	3.00	0.5405	210
	C11	MCPC0038	4.52	2.50	0.3971	205
Round 2	C01	MCPC0163	1.42	0.80	0.0551	291
	C02	MCPC0118	1.48	0.80	0.0610	292
	C03	MCPC0043	1.58	0.90	0.1038	274
	C04	N/A				
	C05	MCPC0048	1.86	1.17	0.0650	265
	C06	MCPC0053	1.52	N/A	0.0946	276
	C07	MCPC0058	1.30	N/A	0.0950	275
	C08	MCPC0063	4.14	2.02	0.2752	228
	C09	MCPC0068	3.29	2.33	0.2441	228
	C10	MCPC0073	4.87	3.12	0.4417	215
	C11	MCPC0078	4.86	3.25	0.3746	212
Round 3	C01	MCPC0168	1.04	0.80	0.0443	289
	C02	N/A				
	C03	MCPC0113	1.38	1.00	0.0504	283
	C04	N/A				
	C05	N/A				
	C06	MCPC0103	1.92	1.30	0.0855	261
	C07	MCPC0108	2.5	1.60	0.1099	249
	C08	MCPC0083	3.94	2.30	0.2824	229
	C09	MCPC0088	3.04	1.70	0.2136	233
	C10	MCPC0093	N/A	4.30	0.5772	228
	C11	MCPC0098	N/A	2.70	0.4249	218

Figure 17 plots FOMs versus Conditions IDs, and it shows the trend is consistent for the three rounds shown in Table 2. This consistency is mainly due to the fact that the grain sizes are similar under the same conditions in the three rounds, i.e., three rounds of builds produced specimens with similar microstructures, and the microstructures depended on the build

conditions. Since FOMs are related to grain sizes, as shown in Figure 16, they are therefore related to conditions as well.

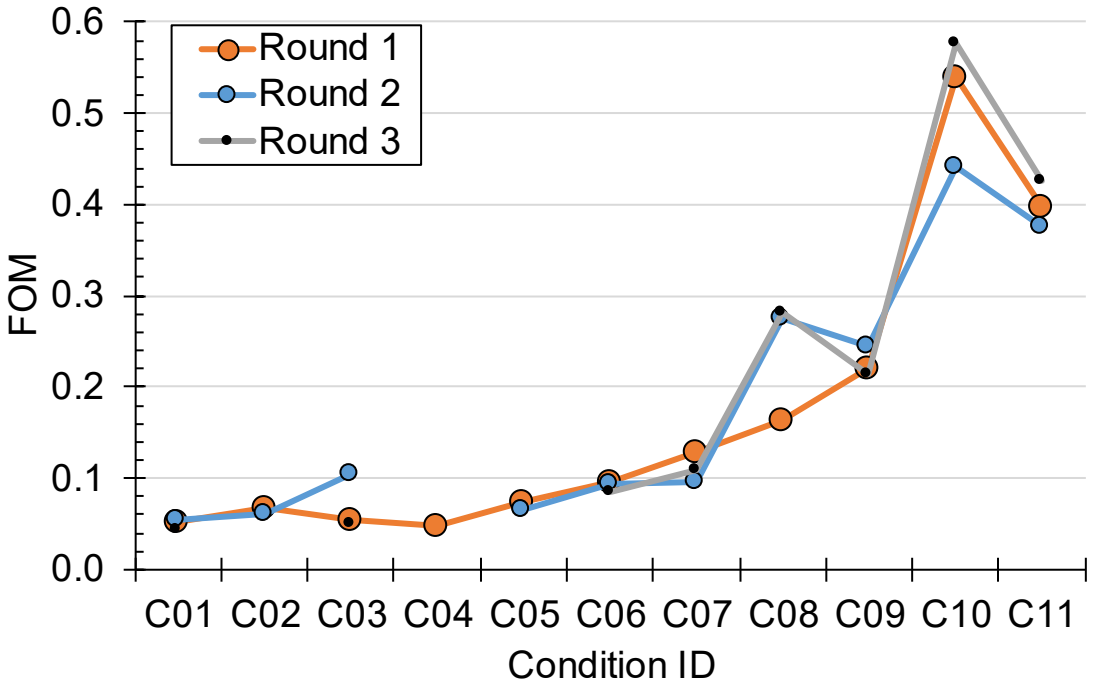

Figure 17. Measured backscattering (FOM) vs. Condition ID.

Figure 18 presents the results of the FOM measurements versus grain sizes based on the CED method as provided from EBSD. The results also show a strong correlation between the ultrasonic backscattering measurements and CED-based grain sizes, similar to intercept-based grain sizes shown in Figure 16. The fitting of the data points is in a slightly different power law than 1.5, and it might be due to different measurement errors for intercept-based grain sizes calculations and for CED-based grain sizes calculations. More studies are needed to find out the exact reason for this discrepancy, but they are beyond the scope of this project. The correlation between FOMs and CED-based grain sizes can be used to deduce CED-based grain sizes from ultrasonic FOM measurements, as demonstrated in Section 5. In the experiment since 20 MHz probe was used the wavelength of shear wave is around 150 microns, far greater than the grain sizes studied. If wavelength is greater than grain size, it is called Rayleigh scattering region. The method in this study is expected to be applicable in this scattering region.

Figure 19 presents the results of the FOM measurements versus microhardness. A strong correlation can be seen between these two measurements as evidenced by the trend line. This is an example showing that the material mechanical properties are directly related to its ultrasonic properties. In the NDE field ultrasonic measurements are already used to measure the mechanical properties, such as hardness, of a material. Note that use of a power fit for the trend line is empirical with no referenced basis.

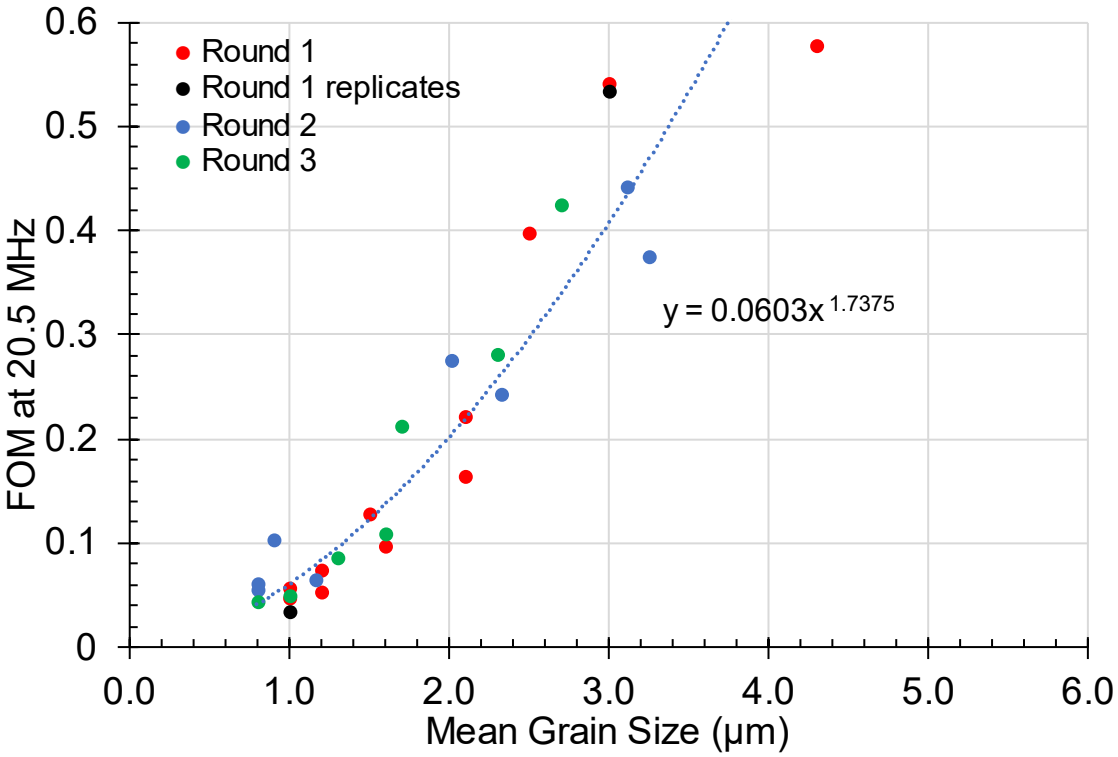

Figure 18. Measured backscattering (FOM) vs. grain sizes (CED).

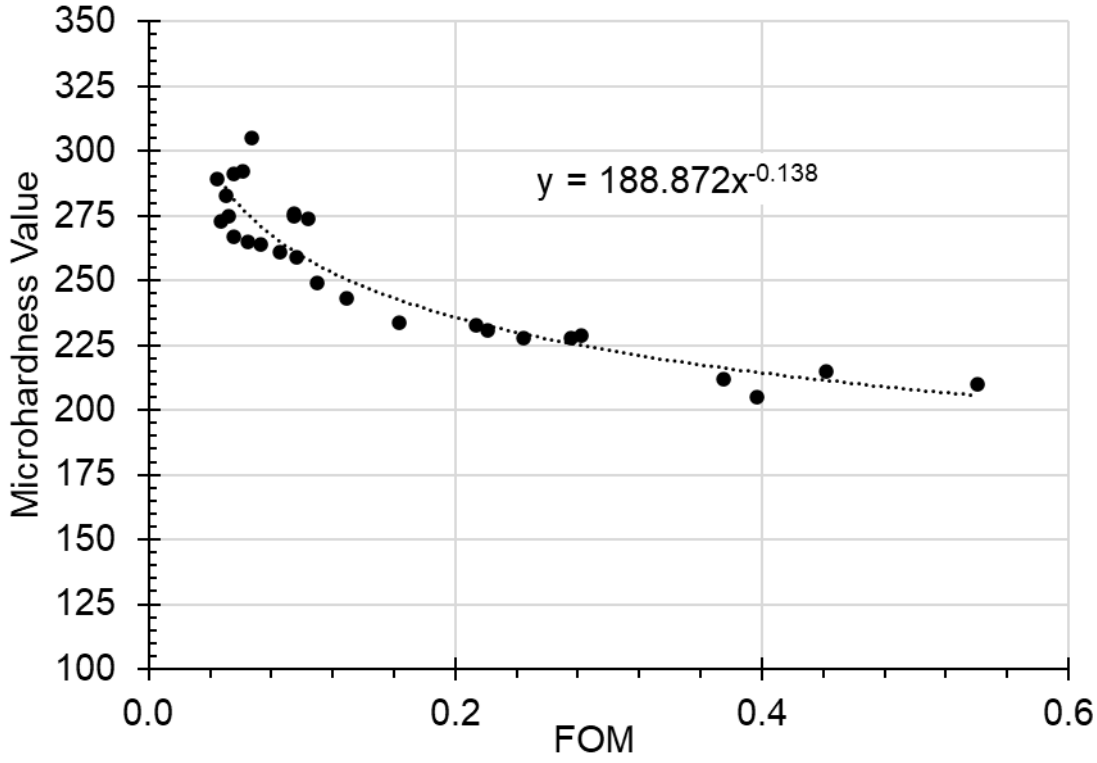

Figure 19. Measured backscattering (FOM) vs. microhardness.

Figure 20 presents the Hall-Petch Relationship, i.e., the measured microhardness versus 1/√CED, that shows that hardness is controlled by material microstructure such as grain sizes that also affect ultrasonic FOMs evidenced in Figure 18.

Together, the relationships in both Figure 19 and Figure 20 can be used to deduce CED from measured FOM. The process works as follows. First, the fit equation in Figure 19 is used to find hardness value from a measured FOM value. Secondly, the fit equation in Figure 20 is used to find CED-based diameter from the hardness value. The method will be demonstrated in Section 5 for the End-to-End Demonstration specimens. A note of caution is that because the fit in Figure 19 is strictly empirical, hence it is probably only valid for the data range that was used.

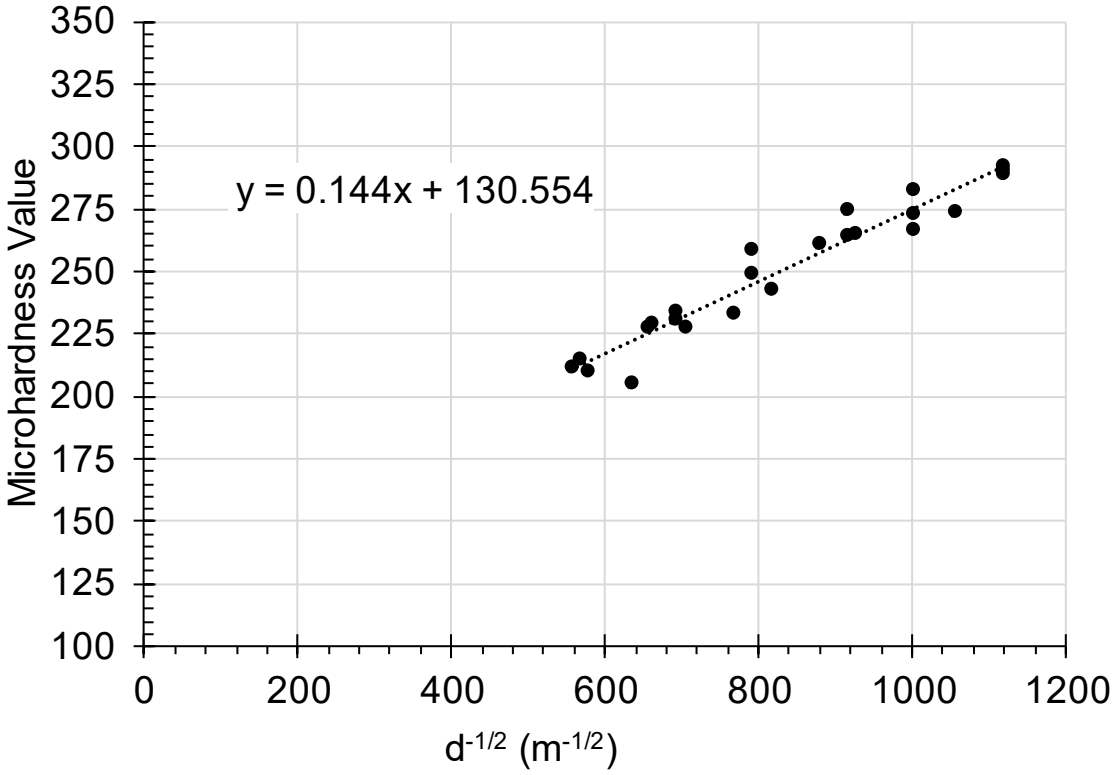

Figure 20. Hall-Petch Relationship, i.e., measured microhardness vs. 1/√CED.

5.0 End-to-End Demonstration

This section presents the results of the E2E demonstration. The purpose is to demonstrate the ability of ultrasonic NDE for measuring grain sizes of materials produced by solid-phase processing techniques, such as FSP and shear-assisted processing and extrusion (ShAPE) techniques. The results in previous sections that correlate ultrasonic measurements to grain sizes and hardness are used to predict the grain sizes of the E2E specimens.

Four specimens were made with four different FSP conditions with condition IDs CID21, CID22, CID23, and CID24. With the same procedures described in Section 4.0, the specimens were scanned first with UT before their grain sizes were measured by the EBSD method. Their FOMs were then calculated, their hardness values were measured, and their grain sizes were deduced based on the relations established in Figures 16, 18, 19, and 20.

Figure 21 shows an example B-Scan for each specimen. On the right side of each B-Scan, a sketch shows the location of the window inside which the ultrasonic data will be processed to calculate FOM. C21 specimen and C23 specimen have significant trenches due to extreme FSP conditions in unsteady state that caused irregularities on the B-Scan images that can distort grain size predictions, so the areas used for ultrasonic data processing will stay away from them, as shown as the black dashed box on the left side image and the blue solid box on the right-side sketch.

Figure 22 shows the five locations where EBSD measurements were done for grain sizes, including L01, L02, L03, L04, and L05. Among them, L02 and L04 are roughly within the area where ultrasonic data were processed to predict grain sizes, so the mean grain sizes by EBSD were calculated as the average of L02 and L04.

Table 6 lists the E2E results from (Todd et al. 2024d), including the UT FOMs for four specimens, the predicted hardness values from fit of Figure 19, the predicted CEDs from Hardness-CED fit of Figure 20 using the predicted hardness values, the predicted CEDs from FOM-CED fit of Figure 18, the measured hardness values near L02 location, the EBSD measured mean CED for L02 and L04 locations, the predicted intercept-based grain sizes from FOM-Intercept fit of Fig. 16, and the measured mean intercept-based grain sizes from the EBSD grain boundary images. The predicted hardness values are close to the measured hardness values by microhardness measurements, and the predicted CEDs are close to the measured CEDs. Note that the intercept-based grain sizes from EBSD for C23 and C24 are questionable because their grain boundary images contain less than 30 grains in any direction, short of the 50 grains required for the intercept method.

Figure 23 presents the results of the FOM measurements versus grain sizes based on CED method, with E2E results being added to the Rounds 1, 2, and 3 results.

The E2E results indicate that ultrasonic backscattering measurements can be used to accurately measure CED grain sizes and hardness. The predicted CEDs have a good agreement with the EBSD results, better than the predicted intercept grain sizes do. These limited cases suggest that ultrasonic backscattering measurements have potential for measuring grain sizes of materials with ultrafine grains produced by SPP techniques. More studies are needed to determine how reliable and predictive the method is. The four blind specimens in this study had CEDs above 2.4 microns. More blind specimens should be studied to verify the method, including specimens whose CEDs are below 2.4 microns and go down to one micron. It’s also desirable to study uncertainties for both of ultrasonic measurements and

EBSD measurements so that the confidence level of predicting grain sizes with ultrasonic measurements could be quantified.

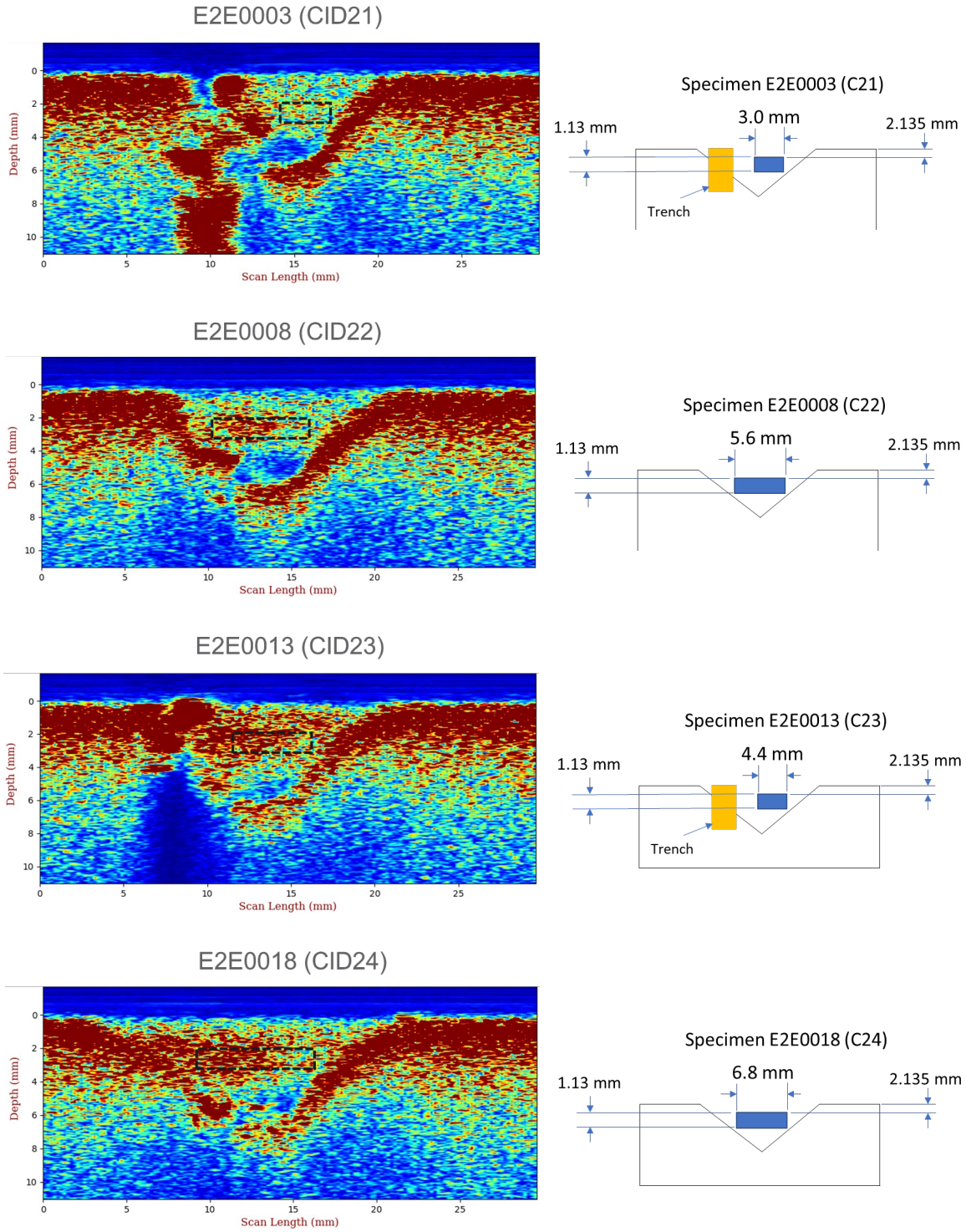

Figure 21. Example B-Scans of E2E specimens and their data processing zones.

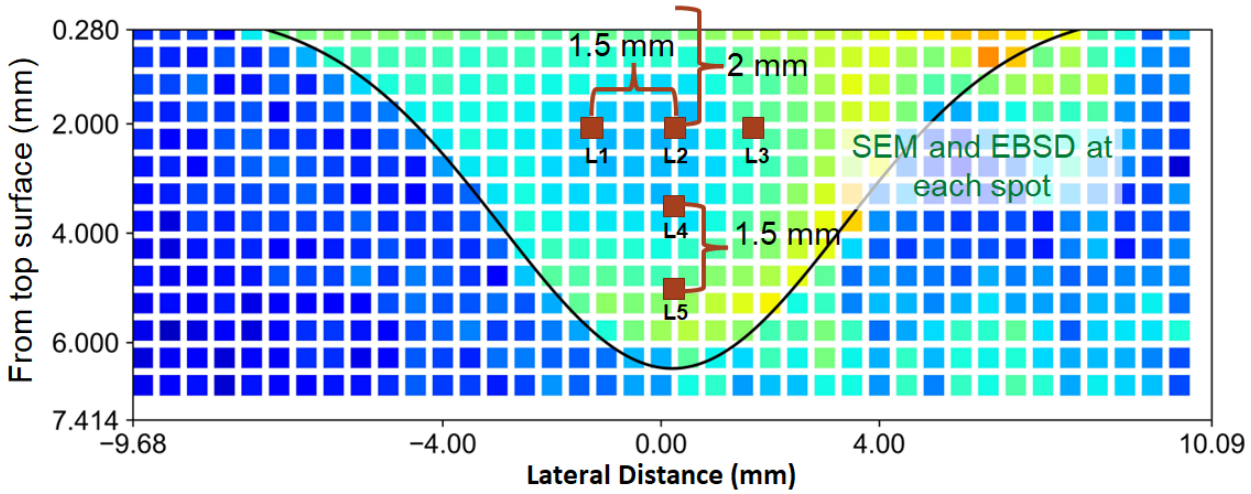

Figure 22. Locations where mean CED is calculated.

Table 6. E2E results.

FSP Condition ID	Specimen ID	UT FOM @20.5 MHz	Hardness from fit of Fig. 19	Hardness (near L02)	CED from Hardness-CED fit of Fig. 20	CED from FOM-CED fit of Fig. 18	Mean CED for L02 and L04	Intercept grain size from fit of Fig. 16	Intercept grain size from EBSD
C21	E2E0003	0.2782	226	225	2.3	2.4	2.4	3.8	5.0
C22	E2E0008	0.3946	215	212	2.9	2.9	2.6	4.7	5.2
C23	E2E0013	0.5835	204	205	3.8	3.7	3.7	6.0	8.1*
C24	E2E0018	0.5314	207	197	3.6	3.5	4.2	5.7	8.6*

*The number of grains on the grain boundary images was low and may have biased the results.

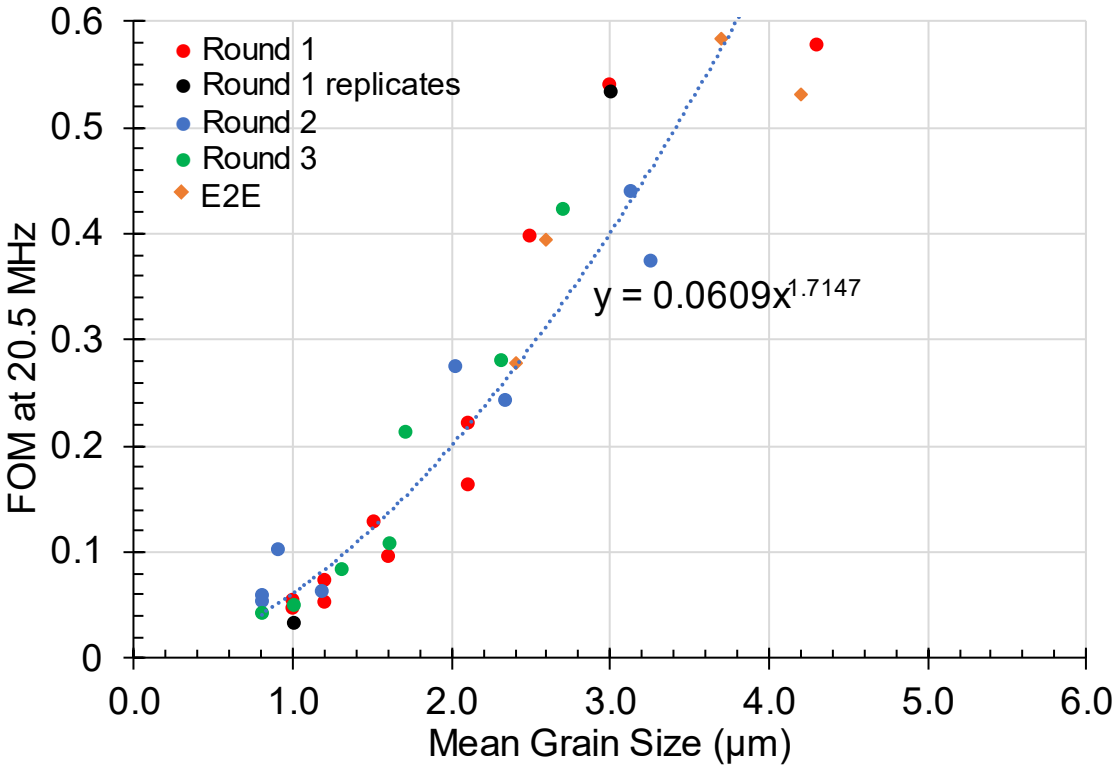

Figure 23. Measured backscattering (FOM) vs. grain sizes (CED), including E2E results.

6.0 Conclusions

A process was established in the laboratory to characterize 316L stainless steel, which is an example of polycrystalline metal made by solid-phase processing such as FSP using ultrasonic NDE methods. It was demonstrated that ultrasonic NDE could be used to detect manufacturing defects produced during the friction stir processing. A procedure was developed to measure ultrasonic backscattering coefficients as a function of frequency, and a FORTRAN program was developed to analyze the acquired data to extract backscattering coefficients in terms of FOM. The results showed that the FOM and grain size are highly correlated. It was also shown that the FOM and microhardness are highly correlated. These results show the potential of ultrasonic NDE for characterizing the microstructure of stainless-steel materials with ultrafine grains (as small as 1 μm) usually produced by FSP and ShAPE. The subsequent E2E demonstration successfully predicted the grain sizes of four FSP specimens.

With the established capability described here, opportunities to further refine the process and apply the capability to meet our sponsors' practical needs can be pursued. In the current work, grains are equiaxed and the material is considered texture-free. In the future work, elongated grains with preferred crystallographic orientations will be considered, and techniques will be developed to include these microstructural characteristics. Further work is also needed to mature the current techniques for actual field applications, such as in-situ monitoring of solid-phase processing or other advanced manufacturing techniques. This requires automated and faster ultrasonic scanning of materials and other ultrasonic scanning techniques that will not need liquid couplants, such as laser ultrasound.

7.0 References

Ahmed, S. and R. B. Thompson. 1995. “Influence of Columnar Microstructure on Ultrasonic Backscattering.” In Review of Progress in QNDE, 14B:1617-1624.

ASTM Standard E112-13. 2021. *Standard Test Methods for Determining Average Grain Size*., ASTM Committee E04 on Metallography. doi: https://www.doi.org/10.1520/E0112-13R21.

Gubernatis, J. E., E. Domany, and J. A. Krumhansl. 1977. “Formal Aspects of the Theory of the Scattering of Ultrasound by Flaws in Elastic Materials.” *J. Appl. Phys.* 48: 2804-2811.

Guo, Y., R. B. Thompson, and F. J. Margetan. 2003. “Simultaneous Measurement of Grain Size and Shape from Ultrasonic Backscattering Measurements Made from a Single Surface.” In *Review of Progress in QNDE*, Vol. 22, 2003.

Margetan, F. J., and R. B. Thompson. 1992. “Microstructure Noise in Titanium Alloys and Its Influence on the Detectability of Hard-Alpha Inclusions.” In *Review of Progress in QNDE,* 11B:1717-1724.

Margetan, F. J., R. B. Thompson, and I. Yalada-Mooshabad. 1993a. “Modeling Ultrasonic Microstructural Noise in Titanium Alloys.” In *Review of Progress in QNDE*, 12B:1735-1742.

Margetan, F. J., R. B. Thompson, I. Yalada-Mooshabad, and Y.K. Han. 1993b. “Detectability of Small Flaws in Advanced Engine Alloys”. *Iowa State University Center for NDE Project Reports*: 75-76. https://lib.dr.iastate.edu/cnde_reports/3/.

Margetan, F. J., T. A. Gray, and R. B. Thompson. 1991. “A Technique for Quantitatively Measuring Microstructurally Induced Ultrasonic Noise.” In *Review of Progress in QNDE,* 10B:1721-1728.

Olympus. 2024. “Ultrasonic Flaw Detection Tutorial: 2.3 Wave Propagation”, URL: https://www.olympus-ims.com/en/ndt-tutorials/flaw-detection/wave-propagation, accessed on June 3, 2024.

Rose, J. H. 1991. “Ultrasonic Backscattering from Polycrystalline Aggregates Using Time-Domian Linear Response Theory.” In *Review of Progress in QNDE,* 10B:1715-1720.

Rose, J. H. 1992. “Ultrasonic Backscattering from Microstructure.” in *Review of Progress in QNDE,* 11B:1677-1684.

Rose, J. H. 1993. “Theory of Ultrasonic Backscattering from Mutiphase Polycrystalline Solids.” In *Review of Progress in QNDE,* 12B:1719-1726.

Smith, E. L. 2021. LDRD Project 79593 (AGILE) Project Management Plan Lite.

Stanke, F. E. and G. S. Kino. 1984. “A Unified Theory for Elastic Wave Propagation in Polycrystalline Materials.” *J. Acoust. Soc. Am.* 75:665-681.

Todd D.R., K. Nwe, M. Pole, Y. Guo, A.D. Guzman, A. Ortiz, and M.J. Olszta, et al. 2024a. *Materials Characterization, Prediction, and Control Project; Summary Report on Material Characterization, Part 1*. PNNL-36768. Richland, WA: Pacific Northwest National Laboratory.

Todd D.R., K. Nwe, M. Pole, Y. Guo, A.D. Guzman, A. Ortiz, and M.J. Olszta, et al. 2024b. Materials Characterization, Prediction, and Control Project; Summary Report on Material Characterization, Part 2. PNNL-36963. Richland, WA: Pacific Northwest National Laboratory.

Todd D.R., K. Nwe, M. Pole, Y. Guo, A.D. Guzman, A. Ortiz, and M.J. Olszta, et al. 2024c. Materials Characterization, Prediction, and Control Project; Summary Report on Material Characterization, Part 3. PNNL-36964. Richland, WA: Pacific Northwest National Laboratory.

Todd D.R., K. Nwe, M. Pole, Y. Guo, A.D. Guzman, A. Ortiz, and M.J. Olszta, et al. 2024d. Materials Characterization, Prediction, and Control Project; Summary Report on Material Characterization, Part 4. PNNL-36965. Richland, WA: Pacific Northwest National Laboratory.

Appendix A — Investigation of Grain Size Measurement Techniques for Friction Stir Processed Austenitic Materials

Following is an unpublished work that demonstrates the performance of the MATLAB program discussed at the end of Section 2.1 for determining intercept-based grain sizes.

INVESTIGATION OF GRAIN SIZE MEASUREMENT TECHNIQUES FOR FRICTION STIR PROCESSED AUSTENITIC MATERIALS

D.A. Koch
Pacific Northwest National Laboratory
Richland, WA

J.D. Escobar
Pacific Northwest National Laboratory
Richland, WA

Y. Guo
Pacific Northwest National Laboratory
Richland, WA

D.R. Todd
Pacific Northwest National Laboratory
Richland, WA

L.E. Smith
Pacific Northwest National Laboratory
Richland, WA

E. Barker
Pacific Northwest National Laboratory
Richland, WA

ABSTRACT

Multiple techniques for grain size measurement are compared for friction stir processed type 316L austenitic material. Two software methods of grain boundary analysis/mapping are compared: AZtecCrystal and MTEX. These maps are then used to compare three methods of grain size measurement: manual linear-intercept based on ASTM E112, ultrasonic attenuation prediction using a two-point correction function, and the proprietary AZtecCrystal software package. Four grain boundary misorientation thresholds, ranging from 3 to 15 degrees, are investigated across multiple methods.

Keywords: ASTM E112, grain size, ultrasonics, grain boundary threshold

1. INTRODUCTION

Real-time process monitoring using ultrasonics has recently been gaining attention across multiple domains (Chabot et al. 2020; Henning et al. 2006; Javadi et al. 2020) Solid phase processing (SPP) is one such domain, where the close coupling of complex microstructures with processing conditions lends itself to continuous data collection. With enough data, it is possible to dynamically modify process variables to achieve a desired microstructure, or range of microstructures, within a single component. Given the number of variables linking processing with resultant microstructure, machine learning (ML) immediately becomes a viable tool for sifting through the large data sets needed for mapping all casual links.

A first step to generating such data sets has been undertaken using friction stir processed (FSP) type 316L stainless steel specimens. Recorded process parameters were varied along a FSP plate in a stepped fashion, careful to ensure each step contained sufficient plate length under steady-state conditions. Specimens, taken from each step, can then be used to build the data collection needed for the ML algorithm. For this initial data evolution, grain size was selected as the first microstructure condition to map back to processing variables.

While grain size is a logical first step due to its broad contribution across many material properties, estimating the average grain size from microstructures produced via SPP is much more complex when compared to conventional manufacturing cases. During SPP, the convolution of intense shear and frictional and deformation heating result in the formation of refined microstructures via dynamic recrystallization (DRX) mechanisms (Sakai et al. 2014; Heidarzadeh et al.

2021). After FSP of face-centered cubic metals, the typical microstructure consists of finely dispersed DRXed grains (Heidarzadeh et al. 2021; Mishra et al. 2005; Liu et al. 2020) containing residual presence of subgrain boundaries and twin boundaries (Mironov et al. 2015; Escobar et al. 2022). The size and shape of DRX grains strongly depend on the processing conditions, and therefore the final microstructures can be either refined equiaxed grains containing twin boundaries or elongated refined grains with diffuse or no twin boundaries (Mironov et al. 2015; Barmouz et al. 2014). Therefore, FSP microstructures are challenging for ASTM E112 standards given the coexistence of the three main limitations described before (grain size, grain shape, and twin boundaries).

Grain size characterization using EBSD offers a potential solution to these former limitations. EBSD analysis allows for a more accurate differentiation between grain boundaries, subgrain boundaries, and twin boundaries, based on crystallographic misorientation analysis. First, grain and subgrain boundaries can easily be differentiated via misorientation threshold filtering. The misorientation between two grains is typically above 10-15°, whereas the misorientation between subgrains is smaller and typically reported between 2-15° (Jazaeri et al. 2004; Hurley et al. 2003; Humphreys 2004). On the other hand, annealing twin boundaries, also known as coincidence lattice sites (CSL Σ3) can also be identified as these show a characteristic axis-angle pair (~60° on [111]) (Patala et al. 2012).

Grain size quantification based on optical microscopy of etched samples has been widely used in the field of metallurgy. However, one major drawback is that one cannot differentiate between grain boundary types. Therefore, it is unclear whether this methodology is addressing the actual grain size, or if results are skewed by the contribution of false positives, such as subgrains or irregular twin boundaries which also are revealed by etching. EBSD analysis offers a very precise grain size determination by the following criteria: 1) subgrain and twin boundaries can be merged into their respective parent grains; 2) grain areas can be accurately calculated based on the grain perimeter described by the actual grain boundary. Therefore, the effect of subgrain fragmentation and twinning can be deconvoluted and its contributions to hardening can be identified. This methodology offers a unique potential to clarify the contribution of fragment size (subgrains and twins) and boundary misorientation type onto hardness via crystallographic analysis.

For the above reasons, EBSD has been chosen as the sole method for microstructural imaging for this study, from which software grain boundary reconstruction will be generated. The resultant images will be used to compare multiple grain size methods and determine any limitations.

A question that arises when comparing various methods of grain measurement is definitional: what determines a grain? While grain boundaries are two-dimensional defects separating neighboring crystals with different crystallographic orientations, it is important to make proper distinctions between possible types of boundaries. Low angle grain boundaries (LAGB) separate subgrains and are represented by lattice mismatches typically between 2 and 15°; while high angle grain boundaries (HAGB) are defined by a mismatch equal or larger than >15°. Historically, HAGBs have been classified anywhere within the 10-15° range, while LAGBs may start between 2-5°. The presence of subgrains provide a challenging scenario when calculating grain size, as both their inclusion and exclusion could lead to poor correlations with physical properties, depending on the degree of their influence. Therefore, a methodic investigation of the effect of grain boundary misorientation threshold is an important topic to understand grain size and physical property relationships.

This paper sets a foundation for future research, where multiple methods of grain measurement will need to be utilized to investigate the microstructures of FSP specimens. Two methods of grain boundary analysis (threshold detection) are compared using EBSD-generated images. Those maps are used to compare three methods for determining average grain size: manual-count linear intercept, a commercial software package, and a custom-written script that uses a general solution of ultrasonic wave propagation to predict grain size. Limitations of these methods are investigated by varying the thresholds of grain boundary maps from 3-15 degrees.

2. MATERIALS AND METHODS

Eleven specimens were prepared from friction stir processed (FSP) stainless steel plates of 316L stainless steel. The ability of FSP to vary welding parameters in-process, and thereby affect the associated microstructure, allowed for stepped transitions of the microstructure to be formed along a single plate. Real-time monitoring of the process parameters was used to ensure that all specimens were cut from areas exhibiting steady state parameters, and away from any transition zones (Ross et al. 2017). All grain size measurements were taken near the center of the highly processed stir region, away from areas of microstructural transition (see Figure A1).

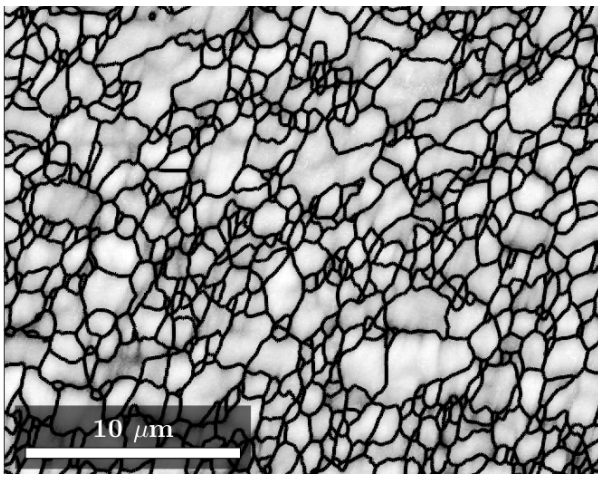

FIGURE A1: TYPICAL MICROSTRUCTURE.

Grain boundary analysis was performed through EBSD using two methods. The initial method used the AztecCrystal (AZtec) software package distributed by Oxford Instruments. The resultant images mapped grain boundaries as black, single-pixel lines, against an otherwise grey scale image. On the other hand, MTEX is a Matlab freeware toolbox that allows for semi-automatic, methodical analysis of EBSD data.

For the MTEX grain boundary analysis, the austenitic phase was indexed using an Cu fcc crystal structure with a 3.645 Å lattice parameter. Low-angle and high-angle grain boundaries were differentiated using the grain boundary reconstruction method proposed by Bachmann et al. (Bachmann et al. 2011). A criterion of misorientation angle of < 15° and ≥ 15°, were used to identify LAGBs and HAGBs, respectively. Annealing twin boundaries were identified as those containing a misorientation of 60° and oriented on [111] by the methodology proposed by Patala, et al. (Patala et al. 2012).

In anticipation of future work where we will assess the correlation between grain size, grain boundary type, and hardness, samples were analyzed using different grain boundary misorientation thresholds. Minimum misorientation angles of 3°, 5°, 10°, and 15° were used to reconstruct all available boundaries which matched such specific angular criteria. This was useful to reconstruct, for example, grains and subgrains (3°), to filter specific subgrains with specific low misorientation angles (>3° and <15°), or to completely suppress the presence of subgrains (15°). Additionally, CSL Σ3 boundaries were identified and accounted as individual sub-regions inside a parent austenitic grain or merged within the corresponding parent grain (>15°) to obtain a shell-only structure.

Three methods for grain size measurement were evaluated, referred to as AZtec, P(x), and E112. The first method utilized the same AZtec software package used to perform the grain boundary analysis above. The second method employed a custom-written software package designed to measure grain sizes consistent with how ultrasound propagates through polycrystalline material. Based on the general solution proposed by Stanke (Stanke et al. 1984), it uses a two-point correction function to estimate the average size of equiaxed grains. The software horizontally scans greyscale grain maps for black grain boundaries, then calculates the probability, P(x), that a line segment of length x is in the same grain. P(x) is then fitted to an exponential function of the form Exp(-x/R), where R is the mean grain radius.

The third method employed the criteria for optical estimation of grain size, as presented in ASTM E112: Standard Test Methods for Determining Average Grain Size (ASTM 2021). The standard contains several methods, notably area methods and linear intercept methods. In area methods, such as the Jefferies method, a circle of known area is used to determine the number of grains per unit area, and then extrapolate the average grain size from there. In the linear intercept method, a line of known length is drawn and the number of grains it intercepts is counted. In both methods, the process is completed several times

and averaged to produce the final grain size estimate. If the material contains equiaxed grains, orientation does not matter. For non-equiaxed grains however, the linear intercept method must be repeated multiple times for each axis of interest.

The linear intercept method, using a series of horizontal lines, was chosen as it better aligned with the horizontal-scanning P(x) method. The test pattern consisted of 5 horizontal lines, each 40 µm in length. In place of the typical mounted, polished, and etched specimens used by Ea2112, consistency was maintained by using the EBSD grain boundary analysis images used by the other two methods.

Comparison of the 3 methods was performed by converting their results to ASTM grain numbers. As 2 of the 3 methods used linear lines (as previously mentioned, it was unclear how AZtec calculated average grain size), and all 3 methods produced an average linear intercept, all calculations were performed using the linear intercept equation from ASTM E112:

$$G = 2LOG_2\left(\frac{320}{l_0}\right) \quad (1)$$

$$l_0 = \frac{L}{N} \quad (2)$$

Where l_0 is the average linear intercept, in µm. This is calculated as the total length of the test lines, *L*, divided by the number of grain boundaries intercepted, *N*. For the P(x) method, which returns the average radius, R, of the grain, it was reasoned that $l_0 \approx R$, since l_0 varies from 0 (a missed intercept) to 2R (the largest intercept distance possible).

3. RESULTS AND DISCUSSION

Initial grain boundary mapping was performed on EBSD images of each specimen using AZtec software. The output was a greyscale image with grain boundaries mapped using black lines approximately one pixel thick. Due to the time required to setup and create these images using AZtec, only one threshold was selected for each specimen. Specimen 1 and 10 used a 3-degree threshold, while the rest used 5 degrees. The resultant grain maps were analyzed using both P(x) and E112 methods, with the results shown in Figure A2.

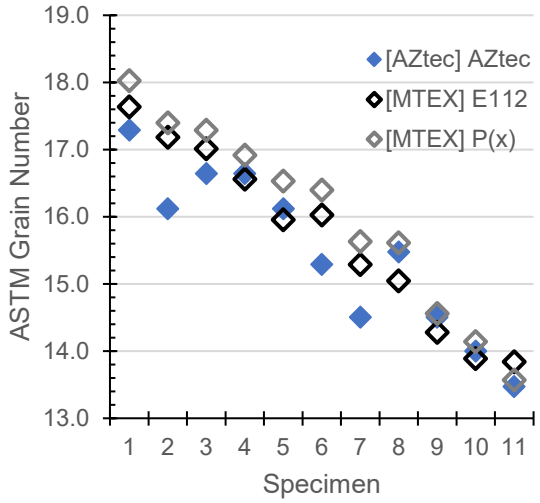

FIGURE A2: AZTEC SOFTWARE-DERIVED GRAIN SIZE COMPARED AGAINST THE E112 AND P(X) METHODS FROM THE MTEX-MAPPED IMAGES. ALL DATA COLLECTED AT 10-DEGREE THRESHOLDS.

The second round of grain boundary mapping was performed on the same EBSD images using MTEX. Grain boundary reconstructions were run over 4 separate thresholds. First, 15 degrees was chosen as representative of the threshold angle commonly selected for grain boundary mapping, while 10, 5, and 3 degrees were selected to reconstruct different types of subgrains. As with the AZtec images, the MTEX-derived images at all 4 thresholds were evaluated using the P(x) and E112 methods. They were compared, both against themselves for internal consistency (Figure A3), and against each other for agreement (Figure A4).

The AZtec and MTEX grain boundary mapping methods were evaluated for agreement by comparing the ASTM grain numbers from their respective P(x) and E112 calculations (Figure A4). The standard deviation between the P(x) grain numbers from both mapping methods was 0.22 while E112 was 0.16.

The Aztec software was also used to calculate grain size. Unfortunately, these were performed at a 10-degree threshold without the requisite greyscale image for analysis by the other methods. Figure A4 shows this AZtec dataset, compared against the P(x) and E112 methods that were performed on the MTEX-derived 10-degree threshold greyscale image. While the underlaying EBSD image was identical in all cases and Figure A4 indicates good alignment between mapping methods, without an

AZtec-produced grain boundary map available for all methods, this data contains additional uncertainty.

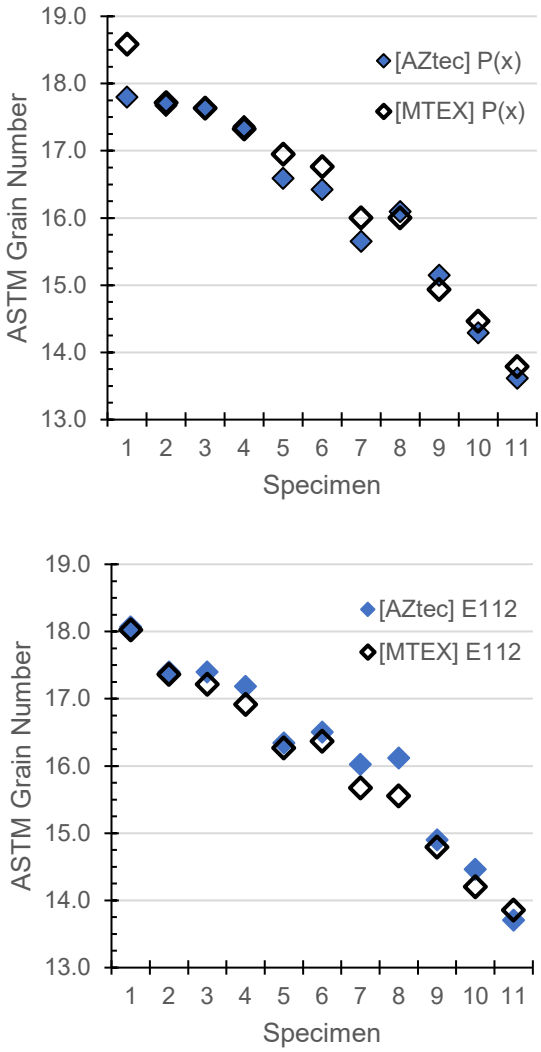

FIGURE A3: COMPARISON OF THE AZTEC AND MTEX IMAGE DERIVED ASTM GRAIN NUMBERS USING BOTH THE (a) P(X) AND (b) E112 METHODS. THRESHOLD USED WAS 5 DEGREES FOR ALL SPECIMENS EXCEPT 1 AND 10, WHICH WA 3-DEGREES.

The E112 method was evaluated for human influence throughout the data collection period. The 5-degree threshold image of specimen 4 was arbitrarily chosen for a periodic recount over the 3-day collection time. In total, this specimen was counted on 10 separate occasions. No counts were successive, with each separated by a minimum of 4 other specimen counts. This separation was done for two reasons: to minimize the chances of successive repeated counts leading to sample familiarization, and to look for any change in counting methodology throughout the collection time. With an average count of 220.9 grains and a standard deviation of 4.5, no bias sufficient to affect the results was observed. The results also fell within the counting accuracy suggested by (Geping, 2020), where up to 2 counting errors per 50 (4%) was considered neglectable.

Both the stand-in method for ultrasonic grain measurement, P(x), and the manual E112 linear intercept method show a high degree of agreement. This agreement is maintained across 4 thresholds, from 2 through 15 degrees. While the results suggest that P(x) produces a slightly higher grain number, without repeat runs to assess measurement error, its statistical significance remains uncertain. When comparing grain number at different thresholds within each method, the uniform shift seen is suggestive of uniformly distributed grain size.

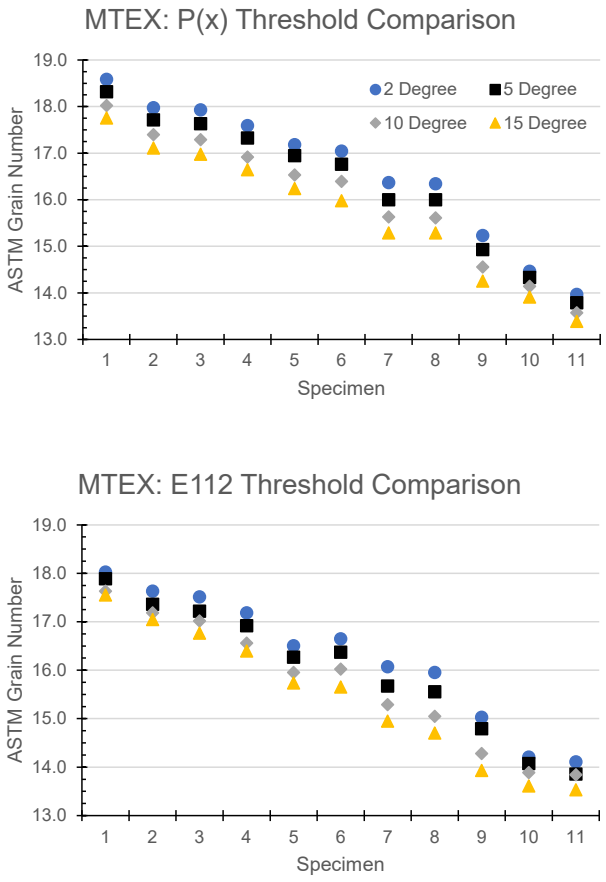

FIGURE A4: P(X) AND E112 METHODS FROM THE MTEX-DERIVED IMAGES. COMPARISON OF THE RESULTS OVER 4 THRESHOLDS.

The agreement between P(x) and E112 methods is likely due, in part, to the use of the same EBSD-derived grain maps for both methods. This study did not compare EBSD-derived grain maps against acid-etched specimens, which would likely be a source of additional error due to the different methods that each uses to form their resultant grain maps. This is especially relevant when comparing modern EBSD results against existing literature from the era before widespread EBSD.

Two methods of thresholding were compared, with the results from AZtec and MTEX showing excellent agreement. This suggests that different methods of EBSD-derived grain mapping should produce similar results for a given microstructure and threshold.

The AZtec grain measurement method showed the most deviation from other methods. There are three sources of error that could explain this. The first source of error could be the use of MTEX-derived grain maps for the comparison methods. As previously mentioned, this was due to a lack of AZtec-derived grain maps at the appropriate thresholds. Given the cost to produce them, and high degree of alignment already seen between the grain mapping methods, it was decided to proceed with the existing data and note the discrepancy.

The second possible source of error with the AZtec method could be the presence of non-equiaxed grains. Both the P(x) and E112 methods assumed equiaxed grains and made their measurements only horizontally. While it is unknown how the AZtec software calculated grain size, it is likely that it performs measurements from multiple directions to obtain an accurate average grain size regardless of grain symmetry. If non-equiaxed grains were present, the AZtec method could have conceivably caught it while the other methods missed it.

The third possible source of error could be in how AZtec addresses grain size distributions. Grain size distribution can be important in addition to grain size number as larger distributions (and hence more large grains) tend to be softer than narrow distributions at the same grain size (Morris, 1959). While, there is no consensus on what constitutes too large of a distribution, the AZtec grain measurement software could contain protocols for filtering grain size beyond a certain sigma from the average in order to not skew the results. Since the other methods contained no such protocols, the presence of one with AZtec would lead to differing results.

4. CONCLUSION

Both the stand-in method for ultrasonic grain measurement, P(x), and the manual E112 linear intercept method show a high degree of agreement.

5. REFERENCES

ASTM. (2021). *Standard Testing Methods for Determining Average Grain Size*. E112-13. ASTM International.

Bachmann, F., R. Hielscher, and H. Schaeben (2011). *Grain detection from 2d and 3d EBSD data-Specification of the MTEX algorithm.* Ultramicroscopy, 2011. **111**(12): p. 1720-1733.

Barmouz, M., M.K.B. Givi, and J. Jafari (2014). *Evaluation of Tensile Deformation Properties of Friction Stir Processed Pure Copper: Effect of Processing Parameters and Pass Number.* Journal of Materials Engineering and Performance, 2014. **23**(1): p. 101-107.

Chabot, A., et al. (2020). *Towards defect monitoring for metallic additive manufacturing components using phased array ultrasonic testing.* Journal of Intelligent Manufacturing, 2020. **31**(5): p. 1191-1201.

Escobar, J., et al. (2022). *Heterogenous activation of dynamic recrystallization and twinning during friction stir processing of a Cu-4Nb alloy.* Journal of Alloys and Compounds, 2022. **928**.

Geping, B., Et al. (2020). *Evaluation of Uncertainty in Determining Average Grain Size by ASTM E112 Standard*. IOP Conference Series. Mater. Sci Eng. 733 01045.

Heidarzadeh, A., et al. (2021). *Friction stir welding/processing of metals and alloys: A comprehensive review on microstructural evolution.* Progress in Materials Science, 2021. **117**.

Henning, B. and J. Rautenberg (2006) *Process monitoring using ultrasonic sensor systems.* Ultrasonics, 2006. **44**: p. e1395-e1399.

Humphreys, M.H.F.J. (2004). *Recrystallization and Related Annealing Phenomena*.

Hurley, P.J. and F.J. Humphreys (2003). *The application of EBSD to the study of substructural development in a cold rolled single-phase aluminium alloy.* Acta Materialia, 2003. **51**(4): p. 1087-1102.

Javadi, Y., et al. (2020). *Continuous monitoring of an intentionally-manufactured crack using an automated welding and in-process inspection system.* Materials & Design, 2020. **191**: p. 108655.

Jazaeri, H. and F.J. Humphreys (2004). *Quantifying recrystallization by electron backscatter diffraction.* Journal of Microscopy, 2004. **213**: p. 241-246.

Liu, X.C., et al. (2020). *Effect of Stacking Fault Energy on the Grain Structure Evolution of FCC Metals During Friction Stir Welding.* Acta Metallurgica Sinica-English Letters, 2020. **33**(7): p. 1001-1012.

Mironov, S., et al. (2015). *Microstructural evolution of pure copper during friction-stir welding.* Philosophical Magazine, 2015. **95**(4): p. 367-381.

Mishra, R.S. and Z.Y. Ma (2005). *Friction stir welding and processing.* Materials Science & Engineering R-Reports, 2005. **50**(1-2): p. 1-78.

Morris, P.R. (1959). *Comparative Measurements of the Velocity of Propagation of an Ultrasonic Pulse in Uranium Fuel Elements*. AEC Research and Development Report. National Lead Company of Ohio. NLCO-764.

Roney, R.K. (1950). *The Influence of Metal Grain Structure on the Attenuation of an Ultrasonic Acoustic Wave*. Ph.D. Thesis. California Institute of Technology.

Ross, K., et al. (2017). *Simultaneous Independent Control of Tool Axial Force and Temperature in Friction Stir Processing*. in *Friction Stir Welding and Processing IX*. 2017. Springer.

Sakai, T., et al. (2014). *Dynamic and post-dynamic recrystallization under hot, cold and severe plastic deformation conditions.* Progress in Materials Science, 2014. **60**: p. 130-207.

Stanke, F.E., Kino, G.S. (1984). *A Unified Theory for Elastic Wave Propagation in Polycrystalline Materials*. Journal of the Acoustical Society of America. 75 (3). March 1984.

Truell, Rohn. (1960). *Ultrasonic Attenuation and the Physics of Solids. Symposium on Physics and Nondestructive Testing*. Argonne National Laboratory. 4-5 October, 1960. (pg 109-126). ANL-6346.

Pacific Northwest National Laboratory

902 Battelle Boulevard
P.O. Box 999
Richland, WA 99354
1-888-375-PNNL (7665)

www.pnnl.gov